Anal. Bioanal. Electrochem., Vol. 11, No. 2, 2019, 211-266

Analytical & Bioanalytical Electrochemistry

www.abechem.com

Review

Cathodic Electrochemical Deposition of Nanostructured Metal Oxides/Hydroxides and their Composites for Supercapacitor Applications: A Review

Mustafa Aghazadeh

Materials and Nuclear Research School, Nuclear Science and Technology Research Institute (NSTRI), P.O. Box 14395-834, Tehran, Iran

*Corresponding Author, Tel.: +98-21-82064289; Fax: +98-21-82064289

E-Mail: maghazadeh@aeoi.org.ir

Received: 13 November 2018 / Received in revised form: 5 January 2019 / Accepted: 12 January 2019 / Published online: 28 February 2019

Abstract- Supercapacitors (SCs) are promising energy sources with high power densities. In the recent years, many efforts have been made to enhance the low energy density of SCs through improvement of the electrode materials. As electrode materials, metal oxides/hydroxides (MOHs) and their composites usually offer high energy densities as a result of their high theoretical capacitances. Up to now, various synthetic methods have been developed for preparing MOHs. In this regards, cathode electrodeposition through base electrogeneration has been intensively used as a one-step simple technique for obtaining various nanostructures of MOHs composites as high-performance SC electrode materials. In this paper, the reports on the fabrication of MOHs-based nanomaterials through the CED method and their super-capacitive abilities have been reviewed.

Keywords- Metal oxides and hydroxides, Electrochemical synthesis, Supercapacitors

1. INTRODUCTION

Nanostructured metal oxides (MOs) in pure, mixed and composite forms have been recently investigated as electro-active materials for supercapacitors, batteries, sensors, catalyst etc. The most commonly studied MOs include ruthenium oxide [1,2], erbium oxide [3,4], samarium oxide [5,6], manganese oxides [7], holmium oxide [8,9], nickel oxide [10,11], ytterbium and

yttrium oxides [12,13], neodymium oxide [14,15], praseodymium oxide [16], europium oxide [17,18], cobalt oxides [19], gadolinium oxide [20,21], zinc oxide [22,23], and cerium oxide [24]. The nano-scale metal hydroxides (MHs) like $Ni(OH)_2$ and $Co(OH)_2$ have been also applied in the above-mentioned applications [25-29]. Among these, charge storage and catalytic applications have been intensively studied [29-34]. Supercapacitors (SCs) or electrochemical capacitors (ECs), are words used to refer to systems that store charge through (i) formation of a double layer around their high surface area (SA) conductive electrodes, and/or undergoing (ii) fast Faradic redox reactions [35]. Recently, SCs or ECs have attracted interest due to their unique characteristics of high power density and long cycle lives, where they can compensate the energy gap between traditional dielectric capacitors and batteries. In fact, SCs can work at very high charge/discharging loads as a results of the fast charge transfer kinetics [36,37]. Electric double layer capacitors (EDLCs) and pseudocapacitors (PCs) are two types of SCs. In EDLCs, energy is stored *via* charge accumulation at the electrode–electrolyte interface, where Faradic redox reactions are mainly responsible for charge storage in PCs [38-40]. As a result, PCs exhibits higher energy densities (amount of energy in a given mass or volume) than EDLCs, which is less than those of Li-based batteries. Therefore, many research studies have been performed on improving the energy density of SCs without reducing their power density and cycling stability. In this regards, MOHs and their composites have proven to be suitable electrode materials for use in PCs [41]. It was clearly proven that MOHs provide higher energy density for SCs than conventional carbon-based electrodes, and better cycling stability or capacity decay than polymer based electrodes [39]. They involve in both mechanisms of charge storage, when applied as SCs electro-active materials i.e. (a) Faradaic redox reactions and (b) charge accumulation at the electrode–electrolyte interface [41].

In this review, we focus on the papers reported about cathodic electrochemical fabrication of pure and composite metal oxides/hydroxides and their applications as electrode materials for SCs, since 2010. Only the nanostructured MOHs prepared through cathodic electro-deposition *via* base (OH^-) generation have been included.

2. CATHODIC DEPOSITION THROUGH BASE ELECTRO-GENERATION

Up now, many solution-based fabrication procedures have been established for preparing the metal oxides/hydroxides (MOHs) at nano-scale [42,43]. For instance, chemical bath deposition, hydrothermal, solvothermal, sol-gel, microwave synthesis, chemical precipitation, and the like have been developed for preparation of MOHs, and a variety nanostructures such as particles, plates, rods, plates, etc. have been fabricated through these methods. Electrochemical methods i.e. both anodic and cathodic depositions (AED and CED) have been also applied for the synthesis of MOHs [44,45]. Electrochemical fabrication presents a facile route for the preparation of nanostructured MOHs with various morphologies [46-60]. Furthermore, composite MOHs nanostructures can be easily obtained with advantages of

simplicity, low preparation temperature, high yield, low cost, and environmental friendliness [61]. In this regards, cathodic electrochemical deposition (CED) *via* base electro-generation has been used to prepare various MOHs [62-65], and CED has introduced as a simple and easy way for MOHs nanomaterials.

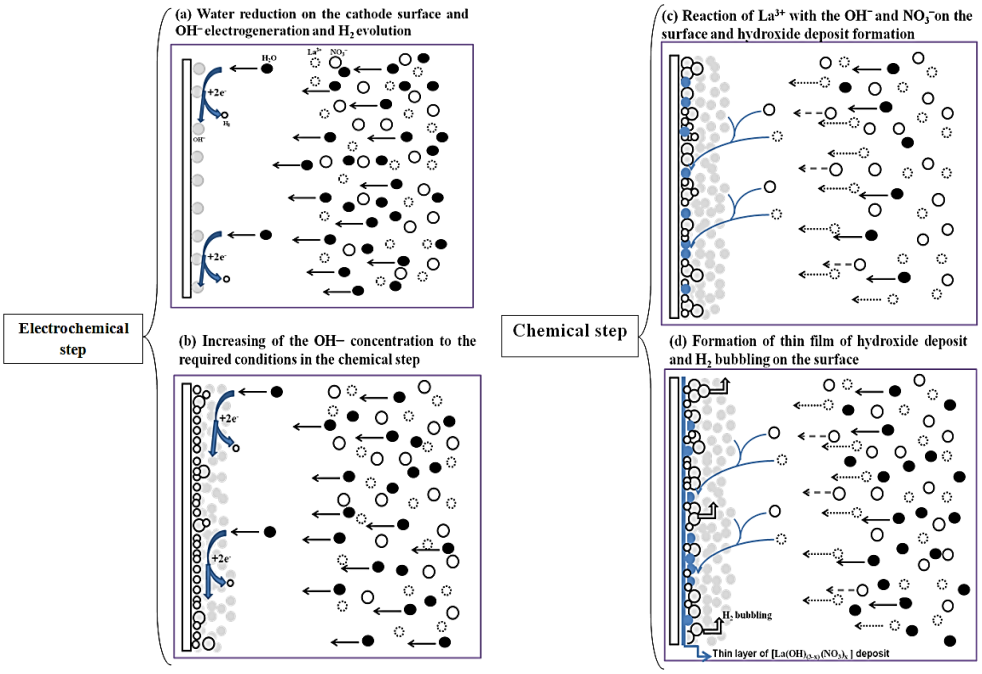

Fig. 1. Schematic view of the $La(OH)_3$ formation steps from nitrate bath (Reproduced with permission from Ref. [84], Copyright 2013, The Electrochemical Society)

For example, we recently used CED for preparation of naked and surface coated iron oxide nanoparticles (IONs) [66-75]. In the cathodic fabrication, hydroxide structure is firstly established on the cathode electrode by chemical reaction of M^{n+} with generated OH^- ions. The fabricated powder is then heat-treated at the suitable temperature and atmosphere to achieve oxide nanostructures [76-80]. Formation of MH on the cathode (from typical aqueous bath containing metal nitrate/chloride salts) has been justified by a two–step mechanism [80-84], as explained below:

Electrochemical step:

$$O_2 + 2H_2O + 4e^- \rightarrow 4OH^- \quad (1)$$

$$NO_3^- + H_2O + 2e^- \rightarrow NO_2^- + 2OH^- \quad (2)$$

$$2H_2O + 2e^- \rightarrow H_2 + 2OH^- \quad (3)$$

Chemical step:

$$M^{n+}(aq) + nOH^-(aq) + yH_2O \rightarrow [M(OH)n\ .yH_2O]\downarrow \quad (4)$$

or

$$M^{n+}(aq) + nOH^-(aq) + xNO_3^- + yH_2O \rightarrow [M(OH)_{(n-x)}(NO_3)_x\ .yH_2O]\downarrow \quad (5)$$

To prepare MO powder, a heat-treatment (HT) step is applied;

$$\text{Hydroxide deposit} \xrightarrow{\Delta} \text{metal oxide product} \quad (6)$$

For example, formation of $La(OH)_3$ *via* the above mentioned two–step mechanism has been described in Fig. 1 [84];

Also, the schematic presenting the $La(OH)_3$ and La_2O_3 nano-rods formation through CED-HT method is provided in Fig. 2 [84]:

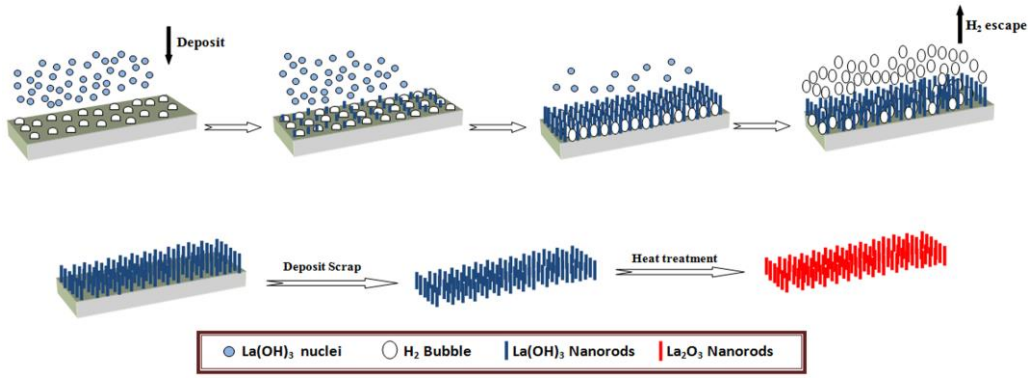

Fig. 2. Schematics of the nucleation and growth of $La(OH)_3$ nanorods, and subsequent calcination step. (Reproduced with permission from Ref. [84], Copyright 2013, The Electrochemical Society)

It is worth knowing that there is no review report on the cathodic deposition of energy nano-materials *via* base generation. Accordingly, we reviewed the published papers on the preparation of metal oxides and hydroxides *via* CED method and their capabilities as the electrodes in supercapacitor applications.

2.1. Cathodic electrodeposition of metal hydroxides

2.1.1. Nickel hydroxide

Among numerous electro-active materials, nickel hydroxide is a promising candidate for use in SCs [85]. $Ni(OH)_2$ has hexagonal-layered crystalline nature and exhibits two crystalline phases of alpha and beta, i.e. α- $Ni(OH)_2$ and β-$Ni(OH)_2$ [86]. α-$Ni(OH)_2$ has a hydroxyl-deficient crystal unit cell with interlayered anions and H_2O molecules, where beta phase has a brucite structure without H_2O molecules. During cycling, α- and β-$Ni(OH)_2$ are converted into γ-NiOOH and β-NiOOH as a results of Faradic redox reactions [86]. For example, in the SC electrode composed of beta phase, the following surface faradic reactions are taken placed [87]:

$$\beta\text{- } Ni(OH)_2 + OH^- \leftrightarrow \beta\text{-NiOOH} + H_2O + e^- \quad (7)$$

α-$Ni(OH)_2$/γ-NiOOH couple presents higher capacitance value with trprvy i00 β-$Ni(OH)_2$/β-NiOOH couple, which is related to the greater change in valence. However, alpha phase of $Ni(OH)_2$ has weak chemical stability in high concentrated alkaline solutions, and it is easily converted into β-nickel hydroxide. The theoretical capacitance of this hydroxide is about 3650 F g^{-1}, which is higher than those of Ni oxide (C=2573 F g^{-1}) [85].

So far both forms of nickel hydroxide (i.e. α- and β-$Ni(OH)_2$) with various morphologies have been prepared by CED method and their SC performances investigated. For example, ultra-fine nanoparticles of nickel hydroxide have been deposited *via* CE deposition from 0.005 M $NiCl_2$ at bath temperature of 10ºC. The prepared fine nanoparticles showed a capacitance value of 740 F g^{-1} in the operating range of 0–0.55 V *vs*. Ag/AgCl [87]. CED of nickel hydroxide films on Ni foil were also reported by Fu *et al.* [88]. The prepared film composed of particle-like α-$Ni(OH)_2$, which exhibited a specific capacitance of 2595 F g^{-1}.

Ag nanowires/$Ni(OH)_2$ nanocomposite electrodes were fabricated through CED [89], and a 93% stability after 3000 cycling, and C=1165.2 F g^{-1} at 3 A g^{-}1 were observed for this composite, which related to the facilitated ion and electron transports as a results of synergism between high conductivity Ag and high capacity $Ni(OH)_2$. The nano-size effects on the super-capacitive properties of the deposited α-$Ni(OH)_2$ were investigated by Wu *et al.* [90]. They found that the performances of the CE deposited α-$Ni(OH)_2$ increased with decreasing the α-$Ni(OH)_2$ crystal size. Oval α-$Ni(OH)_2$ nanoplates with crystal size of 3~5 nm×5~7 nm showed ultrahigh Cs values of 348 mAh g^{-1} and 312.5 mAh g^{-1} at discharge loads of 5 A g^{-1} and 100 A g^{-1}, respectively [90]. Porous sphere-like structures of α-$Ni(OH)_2$ were deposited on stainless steel *via* CE deposition from 0.005 M nickel nitrate bath at T=80 ºC and the discharge capacity of 418 mAh/g for a current load of 100 mA/g after 100 cycles was reported[91].

As mentioned α-$Ni(OH)_2$ suffers from low chemical stability at concentrated basic electrolytes. In this regards, many studies have been carried out through partial substitution of Ni cations in the α-$Ni(OH)_2$ lattice by other M^{n+} cations like Zn^{2+}, Al^{3+}, Y^{3+}, Co, and etc. CED method has been applied for preparation of doped α-$Ni(OH)_2$ electrodes. For example, La^{3+}-doped α-$Ni(OH)_2$ was produced *via* CED , and the discharge capability of 840 F/g with a good cyclic reversibility (about 90%) were observed for this materials [92]. Furthermore, flower-like Zn^{2+}-doped alpha-$Ni(OH)_2$ nanostructure has been synthesized by electrochemical deposition method, and it was observed that electrodes doped with 5% Zn^{2+} provide specific capacitance values of 860 F g^{-1} [93].

Well-dispersed nanoparticles of alpha and beta phases of nickel hydroxide were prepared via CED, and it was noticed that ultrafine α-$Ni(OH)_2$ NPs show better SC behavior as compared with ultrafine β-$Ni(OH)_2$ NPs, which are better reversibility, less positive charging potential, greater discharge capacity, higher proton diffusion coefficient, lower E_a-E_c value, higher $E_{OER}-E_a$, and better cycle life [94]. Aguilera *et al.* [95] reported galvanostatic CE deposition of α-$Ni(OH)_2$ cabbages onto Ti plate, and used as SC electrode, where they calculated specific

capacitance of 1903 F g^{-1} a 1 mA cm^{-2}, energy and power density values of 42.31Wh kg^{-1} and 430Wkg^{-1} for this electrode. β-$Ni(OH)_2$ nanospheres by CED method and used as an electrochemical PCs material [96], which the high specific capacitance (754.5 F g^{-1}at the scan rate of 5 mV s^{-1}) and good cycling life (9.9% capacity decay after 1000 cycles) were observed for this material.

Pulse cathodic electrodeposition was used by Lo *et al.* [97] to fabricate ZnO/$Ni(OH)_2$ nanocomposite, and good specific capacitance of 1830 F g^{-1}, energy density of 51.5 Wh kg^{-1}, and power density of 9 kW kg^{-1} were reported for the composite. Petal-like $Ni(OH)_2$-MnO_x nanosheets were fabricated by electrochemical cathodic co-deposition from Mn^{2+}/Ni^{2+} solutions [98]. These nanosheets, assembled in the symmetric supercapacitor device, led to an energy density of 17.36 Wh kg^{-1} at the power density of 249 W kg^{-1} and 1.8 Wh kg^{-1} at 5.01 kW kg^{-1}, respectively.

Furthermore, the composites of nickel hydroxide with graphene-based materials were also fabricated *via* a CED platform in a one-pot procedure. For instance, cathodic electrodeposition of $Ni(OH)_2$ on the rGO was performed by Yang *et al.* [99], and the composite materials exhibited a specific capacitance of 1700 F/g at 5 A/g and 967 F/g at 20 A/g with an excellent cycling ability. Furthermore, SC electrodes composed of polyaniline-nickel hydroxide [PANI/$Ni(OH)_2$] were fabricated on stainless-steel (SS) substrates using a two-step CED route [100], and the enhanced reversibility and stability of amorphous PANI-$Ni(OH)_2$ electrodes were compared to pure $Ni(OH)_2$ electrode.

Wang *et al.* [101] fabricated a binder-free 3D $Ni(OH)_2$ nanoflakes/graphene/nickel foam electrode though CED, and the observed specific capacitance was 1520 F/g at a high current load of 60 A/g. They related the superior performance of this electrode into the presence of highly conductive graphene layers on the nickel foam, which remarkably promotes the charge transfer at electrolyte/electrode interface and stated that the 3D graphene/nickel foam substrate significantly improves the cycle life of hydroxide film due to the strong adhesion between deposited nano-flakes and graphene film. $Ni(OH)_2$/CMK composite was deposited onto a Ni foam by CED under ambient conditions [102], and compared to the $Ni(OH)_2$@NF electrode, the composite $Ni(OH)_2$/CMK@ NF electrode exhibited a relatively high capacitive ability (Cs=1224 F g^{-1} at 2 A g^{-1}), and low Cs decay (6% after 3000 cycling), which attributed to the electronic and ionic synergism between hydroxide NPs and CMK. Li *et al.* [103] prepared an SC electrode composed of intertwined caterpillar-like NiFe LDHs deposited on rGO/Ni foam (i.e. NiFe LDHs/rGO/NF) [19]. They deposited rGO onto NF at an applied voltage of −1.2V *vs*. SCE, and then the NiFe LDHs were coated onto the formed rGO/NF electrode through CED. The fabricated composite displayed a high specific capacitance of 1462.5 F g^{-1} at a current density of 5A g^{-1} and retained about 64.7% of the original capacitance after 2000 cycles. Using *in-situ* CE electrodeposition, Jiang *et al.* [104] prepared 3D graphene/$Ni(OH)_2$ composites with flower-, slice- and particle-like morphologies, and observed that the nano-

flower composite was capable of providing higher Cs values (718.2 F/g at 6.7A/g in 6.0 M KOH electrolyte) and a good cycle life (84.2% capacitance retention after 500 cycles) compared to nanoparticles and nano-slices. CE deposited $Ni(OH)_2$ onto Ni foam with porous and 3D morphology delivered a Cs of 3152 F g^{-1} at 4 A g^{-1} [105]. Also, nano-flakes grown onto Ni foam (NF)-supported vertically oriented graphene nanosheets (V-GNs) were fabricated using CED and applied as electrode material for supercapacitor electrodes. The $Ni(OH)_2$/GNs/NF electrode exhibited a high Cs of 2215 F g^{-1} at a current density of 2.3 A g^{-1}, enhanced cycling stability and high rate capability [106]. These reports indicate that CED method is a simple technique for fabrication of binder-free pure and/or composite SC electrode based on nickel hydroxide.

2.1.2. Cobalt hydroxide

$Co(OH)_2$-based materials are attractive due to their layered structures and large interlayer spacing, which gives rise to high surface areas and a fast mass transfer rate (i.e. ion insertion/desertion) [107,108]. For SC the electrode composed of $Co(OH)_2$, two plausible reactions can occur as follow:

$$Co(OH)_2 + 2OH^- \leftrightarrow CoOOH + H_2O + e^- \quad (8)$$

$$CoOOH + 2OH^- \leftrightarrow CoO_2 + H_2O + e^- \quad (9)$$

It is well known that cobalt hydroxide shows two crystalline forms of alpha- and beta-$Co(OH)_2$. Alpha phase is metastable and easily transformed into the more stable β-$Co(OH)_2$ in concentrated basic electrolyte. So far, various nanostructures of $Co(OH)_2$-based materials have been fabricated by CED and applied as SC electrode materials, which shall be reviewed here. For example, uniform nano-discs of $Co(OH)_2$ were successfully fabricated by galvanostatic CE deposition from a 0.005M cobalt nitrate bath at 10 °C [109], and a *Cs* value of 736.5 F g^{-1} obtained at the applied voltage of −0.2–0.5 V (*vs*. Ag/AgCl). The authors mentioned that low-temperature CED is a simple way to achieve nanostructured $Co(OH)_2$. Also, nanostructured $Co(OH)_2$ was coated onto electro-etched-carbon fiber (ECF) using cathodic potential route, and a specific capacitance of 1000 F g^{-1} at a discharge load of 3.1A g^{-1} was reported for the $Co(OH)_2$-ECF electrode [110].

Maile *et al.* investigated the effects of different electrolytes and deposition time on the charge storage ability of $Co(OH)_2$ nano-flakes [111]. They prepared nano-flakes using the potentiostatic CED method *via* the NO_3^- reduction reaction on an SS cathode at the optimum deposition time of 30 min, where the deposited $Co(OH)_2$ electrode provided a higher *Cs* value of 276 F g^{-1} in 0.5M KOH electrolyte.

Pulsed CED was used to prepare nanostructures of $Co(OH)_2$. For instance, $Co(OH)_2$ nanocapsules with capacitive performance of *Cs*=1243 F g^{-1} were also prepared *through* this

strategy [112] (Fig. 3). The applied pulse parameters were t_{on}=10 ms, t_{off}=10 ms, i_p=1 mA cm^{-2} and T_{bath}=10 ºC. The proposed mechanism for the formation and growth of the nanocapsules are shown in Fig. 4 [112].

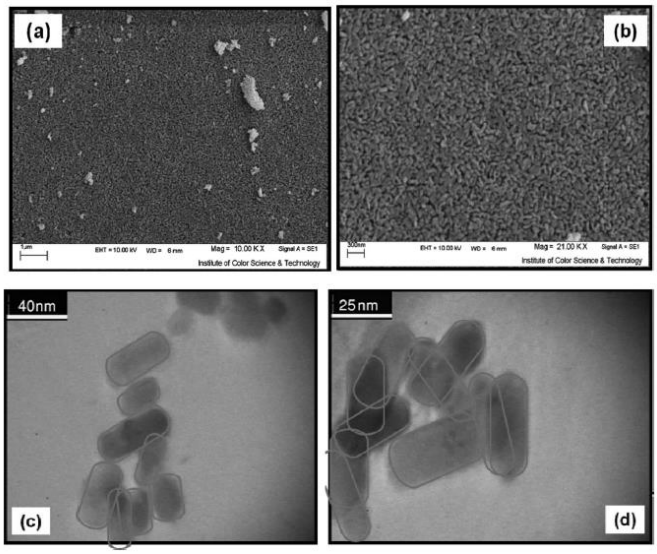

Fig. 3. (a,b) SEM and (c,d) TEM images of the β-$Co(OH)_2$ nanocapsules (Reproduced with permission from Ref. [112], Copyright 2014, The Electrochemical Society)

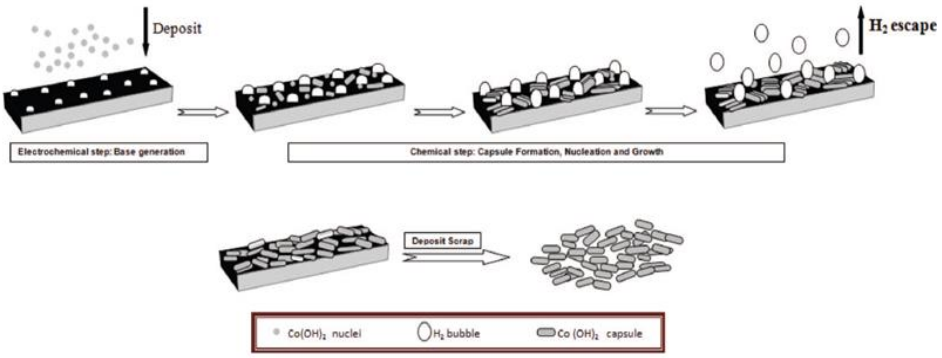

Fig. 4. The formation and growth mechanism of the β-$Co(OH)_2$ nanocapsules (Reproduced with permission from Ref. [112], Copyright 2014, The Electrochemical Society)

Furthermore, pulse current deposition of nanoporous $Co(OH)_2$ films onto Ni foam was reported by Chen *et al.* [113] and the fabricated electrode reportedly exhibited a capacitance value of 1681 F g^{-1} at a current load of 2 A g^{-1} in a potential window of -0.1 to 0.4 V. They reported that pore size and density of the deposited film could be easily tuned by means of pulse parameters.

High surface area sheet- and leaf-like nanostructures of $Co(OH)_2$ were fabricated through cathodic electrodeposition in a 0.005 M $Co(NO_3)_2$ bath at a temperatures of 80ºC and 60 ºC,

respectively [114,115]. The nanosheets and nano-leaves of $Co(OH)_2$ had *Cs* values of 1047.3 F g^{-1} and 772.8 F g^{-1} within the potential range of -0.3 to 0.5 V (*vs.* Ag/AgCl) at the scan rate of 10 mV s^{-1}, respectively. The reports revealed the major role of bath temperature on the deposited cobalt hydroxide, and hence its supercapacitive performance. Pure alpha phase $Co(OH)_2$ were also deposited onto carbon nano-foam by pulsed CED and electrochemical performance of 300 F g^{-1} at current density of 1 A g^{-1} [116]. Recently, ultrafine nanoparticles of β-$Co(OH)_2$ were fabricated by pulse CED from an additive-free nitrate bath [117], where an energy density of 0.105 Wh g^{-1} with Coulombic efficiency of 91.8% were observed for these particles. Mixed $Co(OH)_2$-$Ni(OH)_2$ nanosheets were deposited on an Fe substrate by Jiang *et al.* [118], and the resulting electrode exhibited *Cs* of 853.7 F g^{-1} at 1 A g^{-1} and an 85% capacitance stability at 4 A g^{-1} after 1000 GCD cycles. Using simple pulsed CED procedure, our group prepared uniform $Co(OH)_2$ nanoplates and high Cs of 1012.7 F g^{-1} at of 2 A g^{-1} and an excellent Cs retention (92%) after 1000 cycling were observed [119].

A three component composite based on the cobalt hydroxide i.e. GO/$Co(OH)_2$/chitosan was also reported by CED [120]. The GO/$Co(OH)_2$/chitosan composite exhibited a good specific capacitance of 402 F g^{-1} at 10 mV s^{-1} at the mass loading of 2.6 mg/cm^{-2}. Flake-like $Co(OH)_2$ was deposited from a 0.005 M $CoCl_2$+1 g/L starch bath [121], and the SC electrode developed based on these nanostructure delivered a Cs value of 1125.4 F g^{-1} at a discharge load of 1 g^{-1} and a cycling ability of 80.17% after 2000 GCD at 5 A g^{-1}. Mixed cobalt and nickel hydroxide was coated onto carbon nano-foam paper (CNFP) through cathodic deposition, and the charge storage capability of the $Ni_xCo_{1-x}(OH)_2$/CNFP electrode was tuned by varying the Co/Ni ratios [122]. The optimized stoichiometry was reported to be $Ni_{0.33}Co_{0.67}(OH)_2$, and the electrode showed real capacity/capacitance values of 1.52 C cm^{-1}/2.03 F cm^{-1} at 2.1 mA cm^{-2}.

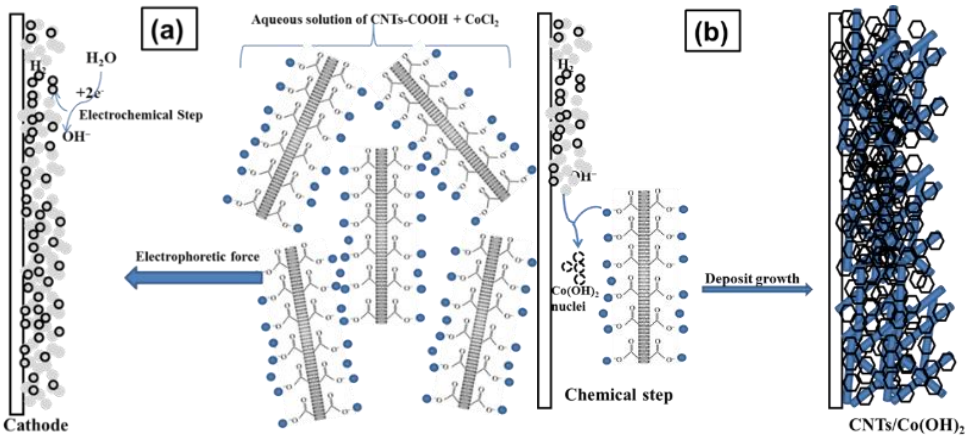

Fig. 5. Schematic view of the formation of $Co(OH)_2$/CNTs nancomposite. (Reprinted with permission from Ref. [124], Copyright 2018 Springer)

Very recently, our group developed a simple one-step CED route for fabrication of a macro-porous 3D β-$Co(OH)_2$/Ni foam from an additive-free 0.005M $Co(NO_3)_2$ electrolyte [123], and *Cs* of 987 F g^{-1} and cycle life of 94.4% were reported for the electrode. Furthermore, a β-$Co(OH)_2$/CNTs nanocomposite was electrodeposited onto a stainless steel (SS) substrate, and used as SC electrode [124]. The $Co(OH)_2$-CNTs/SS electrode delivered a specific capacitance of 1287 F g^{-1} (at 0.5 A g^{-1}), and a capacity decay of 10.6% during 5000 cycles. The co-deposition of β-$Co(OH)_2$/CNTs was fabricated using COOH-functionalized CNTs dispersed in a 0.005M $CoCl_2$ bath. The schematic formation was explained as below [124]:

Zhao *et al.* [125] synthesized $Co(OH)_2$/Ni and $Co(OH)_2$/graphene/Ni foam nano-electrodes by cathodic deposition, and compared their supercapacitive abilities. The $Co(OH)_2$/G/Ni foam showed specific capacitance values of 693.8 and 506.2 F g^{-1} at 2 and 32 A g^{-1}, respectively. It was reported that the *Cs* value of the $Co(OH)_2$/G/Ni foam remained 91.9% after 3000 cycles at 40 A g^{-1}, which was higher than that of $Co(OH)_2$/Ni foam (75.5% Cs retention after 2000 cycles) (Fig. 6). The improvement was attributed to the important role of incorporating graphene in the $Co(OH)_2$ and Ni foam [125].

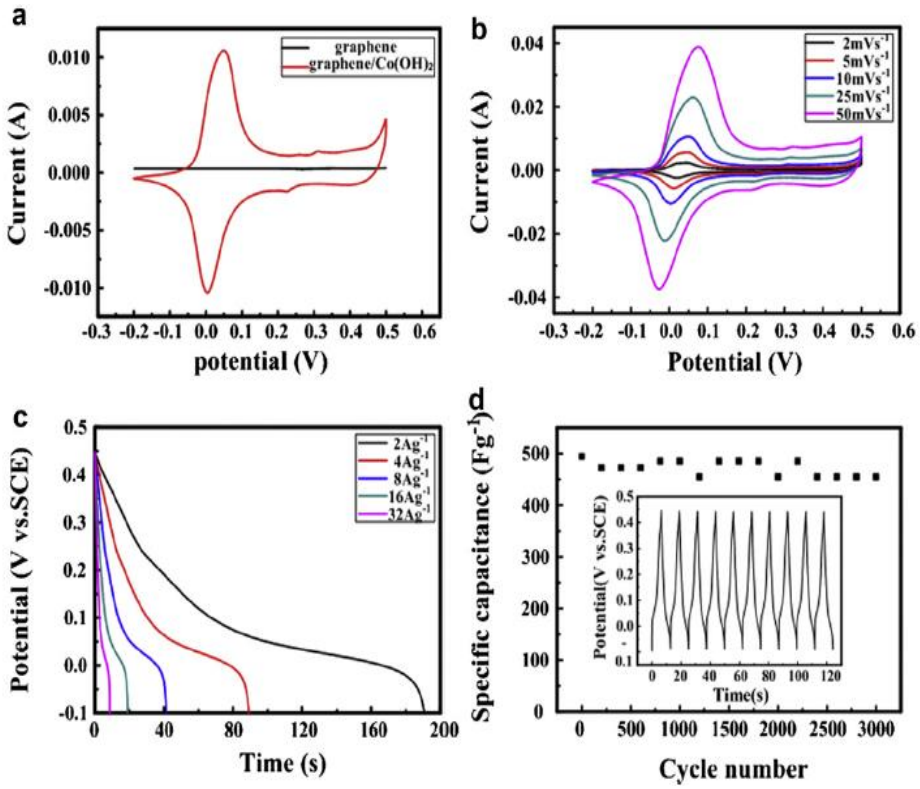

Fig. 6. (a) cyclic voltammograms of $Co(OH)_2$/GNS and GNS on Ni foam at a scan rate of 10 mV s^{-1}, electrochemical properties of $Co(OH)_2$/GNS on Ni foam; (b) cyclic voltammograms at different scan rates; (c) discharge curves at different discharge current densities; and (d) cycling life at charge/discharge current density of 40 A g^{-1}. (Reprinted with permission from Ref. [125], Copyright (2013) Elsevier)

High surface area β-$Co(OH)_2$ nanosheets were also synthesized *through* CED at simple deposition conditions [126], and it was found that the nanosheets were capable to have *Cs* values 886.8 and 734.3 F g^{-1} at the current loads of 1 and 3 A g^{-1}, respectively. Furthermore, nanosheets of α-$Co(OH)_2$ have been fabricated *via* pulsed CED at the same bath used in Ref. [20]), and α-phase nanosheets exhibited *Cs* value of 1122 F g^{-1} at 3 A g^{-1} and a *Cs* stability of 84% after 4000 continues discharging cycles [127]. These reported results verified the importance of applying pulse conditions in the CED synthesis of cobalt hydroxide.

A cobalt hydroxide-polyaniline ($Co(OH)_2$-PANI) hybrid nanocomposite was constructed *via* potentiostatic-deposition method [128], and compared with pure PANI and v electrodes. Cs values of 3.06 F g^{-1}, 215 F g^{-1} and 868 F g^{-1}, respectively, were observed for PANI, HNs and $Co(OH)_2$ in a 1M NaOH electrolyte. And *Cs* stabilities and voltammetric charges of 47%, 60% and 55% (after 1000 cycles) and 17.22 mC cm^{-2}, 836.39 mC cm^{-2} and 1128.73 mC cm^{-2}were reported for the electrodes. The inferior SC performances of composite electrode were explained by the occurrence of inner and outer charges concept [128]. Cheng *et al.* [129] developed graphene–SWNTs and graphene–SWNTs–$Co(OH)_2$ electrodes using CED, and a high energy density of 172 Wh kg^{-1} and a power density of 198 kW kg^{-1} were obtained for composite G/SWNTs-$Co(OH)_2$ electrode.

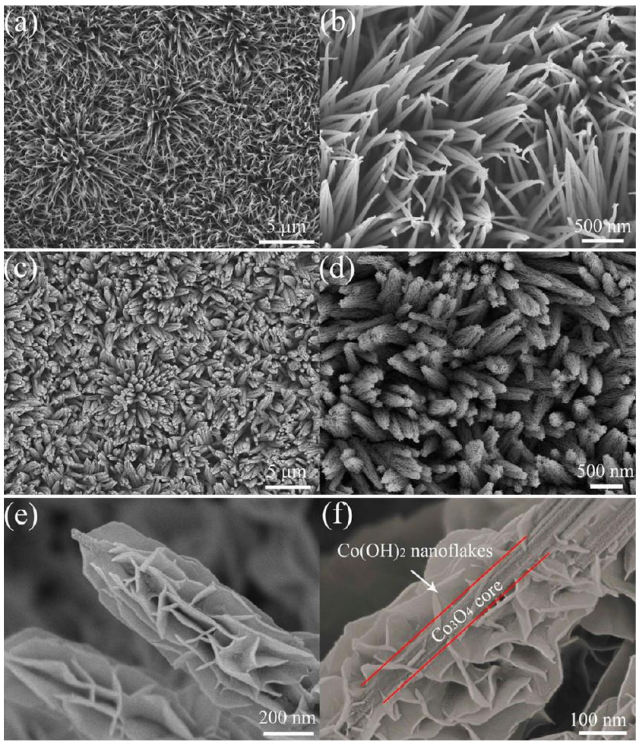

Fig. 7. Electrodeposition of $Co(OH)_2$ nano-sheet branches on Co_3O_4 nanowires. (a,b) SEM images of Co_3O_4 nanowire arrays on nickel foam; (c,d) Co_3O_4/$Co(OH)_2$ core/shell nanowire arrays; (e) Fine view and (f) profile image of a single core/shell nanowire. (Reprinted with permission from Ref. [131], Copyright (2012) American Chemical Society)

They mentioned that SWNTs play the role of a conductive spacer and a conductive binder in the composite electrode. Using CED, α-cobalt hydroxide was established on the rGO-coated carbon fiber paper (rGO/CFP), and the performance of the α-$Co(OH)_2$/rGO/CFP electrodes were studied in basic electrolytes [130]. It was reported that the α-$Co(OH)_2$ structure is deformed at high concentrations i.e., 3-6 M KOH and NaOH, and the optimum concentration of base was 1M [OH^-], in which a Cs value of 1096 F g^{-1} at 1.8 A g^{-1} was exhibited by the α-$Co(OH)_2$/rGO/CFP electrode. Xia *et al.* [131] used CED for fabricating a porous Co_3O_4/$Co(OH)_2$ core/shell nanowire electrode (Fig. 7) with a high Cs value of 812 F g^{-1} at 40 A g^{-1}.

Mesoporous $Co(OH)_2$/$Ni(OH)_2$ nano-sheet networks (NNs) were grown on Ti substrates through a simple CED procedure, and heat-treatment of the prepared electrode resulted in a Co_3O_4/$Ni(OH)_2$ composite mesoporous NNs. The electrode showed a high specific capacitance of 1144 F g^{-1} at 5 mV s^{-1} and good long-term cyclability [132]. Deng *et al.* [133] first electrodeposited a Cu/Ni film onto Ni foam, and then etched copper from the Cu/Ni layer to produce Ni nanotube arrays/Ni foam and sucker-like nanopores Ni/nickel foam, respectively (Fig. 8). Then they cathodiclly deposited $Co(OH)_2$ onto nanoporous Ni substrates (as presented in Fig. 8). The fabricated $Co(OH)_2$@Ni nanotube array and $Co(OH)_2$@sucker-like nanoporous Ni exhibited *Cs* values of 2500 and 2900 F g^{-1} at 1 A g^{-1}, respectively, and an outstanding *Cs* stability of 95% and 92% after 10000 cycles.

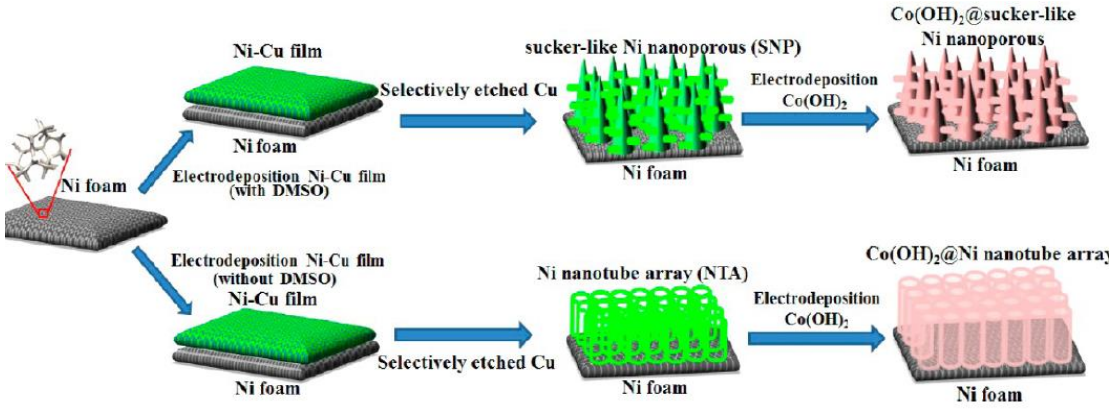

Fig. 8. Scheme of electrochemical preparation of highly porous nanoarchitectured $Co(OH)_2$ electrodes. (Reprinted with permission from Ref. [133], Copyright (2015) American Chemical Society)

A N-methylpyrrolidone (NMP)-assisted CED route was established by Zhao *et al.* [134] to prepare dense layered α-$Co(OH)_2$ nanosheets, and a Cs value of 651 F g^{-1} in a potential range of −0.1 to 0.45 V was observed. α-$Co(OH)_2$ was deposited on CNTs/carbon paper *via* CED and a good specific capacitance value of 1083 F g^{-1} at a 0.83 A g^{-1} in 6 M KOH electrolyte

was obtained [135]. Recently, pure α-$Co(OH)_2$ nanoplates were fabricated using a simple CED procedure and the constructed electrode delivered 781.1 F g^{-1} at 10A g^{-1} with only 10% Cs decay after 3000 cycling [136]. The papers on the fabrication of cobalt hydroxide through CED method revealed the facile formation of α/β-$Co(OH)_2$ composite nanoelectrode by this electrochemical synthetic technique.

2.2. Cathodic electrodeposition of metal oxides

2.2.1. Ruthenium oxide

Various metal oxides have been investigated as SC electrode materials, so far [137-144]. Among them, ruthenium dioxide (RuO_2) is among the most promising candidates for SCs due to its remarkably high specific capacitance (*Cs*=1500–2200 F g^{-1}), good electrical conductivity (~105 S cm^{-1}), a wide practical potential range and a reversible charge-discharge kinetics [145]. In the presence of H^+, RuO_2 exhibited the following charge storage performance [144,145]:

$$RuO_2 + \delta H^+ + \delta e^- \leftrightarrow RuO_{2-\delta}(OH)_\delta \qquad 0<\delta<2 \qquad (10)$$

The ability is responsible for its high theoretical Cs. Cathodic deposition was intensively used by researchers for fabrication of RuO_2-based nano-electrodes. We recently reported the results obtained using RuO_2 nanostructures prepared through CED and their charge storage performances. For example, amorphous and porous RuO_2 thin films were deposited on steel substrates using CED, and a Cs value of 650 F g^{-1} in 0.5 M H_2SO_4 electrolyte was achieved. They found that the SC ability of the RuO_2 electrode was affected by the surface morphology [146]. Li and He [147] fabricated a RuO_2/graphene (RuO_2-ERG) composite onto Ni foam through CE deposition, and a high energy density of 43.8 Wh kg^{-1} at a power density of 0.75 kW kg^{-1} and capacitance retention of 92.8% after 10000 cycles were reported. The authors also prepared a $Co(OH)_2$/RuO_2@Ni foam through a simple CED process [148], and the specific capacitance of 2168 F g^{-1} at 1 A g^{-1} was reported. They found that the performance of the composite electrode increased by 57% and 80% compared to pure $Co(OH)_2$ and RuO_2 electrodes. This improvement was assigned to the good synergism between $Co(OH)_2$ and RuO_2, which guaranteed the shortened ion-diffusion pathways, large surface areas and high electrochemical usage.

Kim *et al.* [149] reported the electrochemical deposition of mesoporous RuO_2 films onto ITO-coated glass substrate from an aqueous $RuCl_3.nH_2O$ bath in the presence of SDS and CTAB as templating agents. They found that the RuO_2 film deposited in the presence of a mixture of SDS and CTAB shows a very high *Cs* (i.e. 503 F g^{-1}), which was 2.6 times higher than Cs of non-porous RuO_2 (i.e. 192 F g^{-1}). These enhancements in RuO_2 performance were related to the higher surface area and facilitated charge transport. Furthermore, the effects of electrodeposition modes on the hydrous RuO_2 electrochemical capabilities were evaluated by

Vishnu Prataap *et al.* [150], and RuO_2 nanostructures with morphologies of particle-, dendrimeric- and mud-cracked morphologies were obtained at the modes of pulse potential, cyclic voltammetry and constant potential, respectively. The nanostructures exhibited *Cs* values of 1180 F g^{-1}, 573 F g^{-1} and 546 F g^{-1} in 0.5 M H_2SO_4 at the scan rate of 5 mV/s, which confirmed the morphology dependent SC performance of RuO_2. Kim *et al.* [151] performed the layer by layer electrodeposition of PANI and RuO_2, and two layered electrodes of electrodeposited RuO_2 ($eRuO_2$) and polyaniline (ePAn) onto Pt were fabricated i.e. ePAn-on-$eRuO_2$/Pt and $eRuO_2$-on-ePAn/pt electrodes. They observed *Cs* values of 810-575 F g^{-1} in the scan rate range of 20-1000 mV s^{-1} for ePAn-on-$eRuO_2$/Pt electrode, where lower *Cs* values of 680-550 F g^{-1} were shown by $eRuO_2$-on-ePAn/Pt electrode. The superior ability of ePAn-on-$eRuO_2$/Pt electrode was devoted to particulate surface and inner pores of the ePAn layer. The effect of deposited film thickness on the SC performance of CED fabricated RuO_2/Ti electrode was reported by Pak *et al.* [152], and a maximum *Cs* of 788 F g^{-1} was achieved at the electrode thickness of 0.0014 g cm^{-2}. Hydrous ruthenium oxide with a tubular morphology was successfully synthesized, through CED, onto Si micro prominence templates, and used as a 3D MEMS microelectrode (Fig. 9) [153]. A specific geometric capacitance of 99.3 mF cm^{-2} was observed after 2000s deposition. A micro-supercapacitor constructed by two identical RuO_2/Si MEMS electrodes delivered a good specific capacitance (23 mF cm^{-2}) and a specific power density (5.4 mW cm^{-2}).

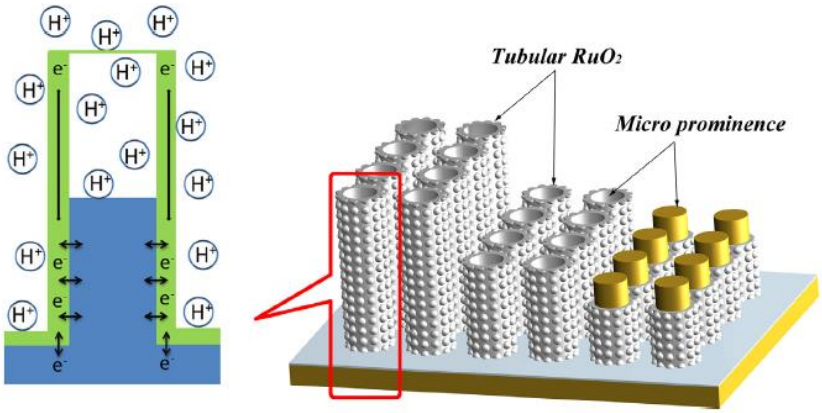

Fig. 9. Desired schematic structure for the tubular $RuO_2.xH_2O$ microstructure applied in a micro-supercapacitor. (Reprinted with permission from Ref. [153], Copyright (2004) Elsevier)

CED accompanied with H_2-evolution was used to prepared a porous hydrous RuO_2 film, and the obtained 3D porous hydrous RuO_2 showed good Cs performance of 809 F g^{-1} at 1.5 A g^{-1}, and a high energy density (112 Wh kg^{-1}) [154]. Furthermore, RuO_2 has electrodeposited onto electro-spun TiO_2 nanorods through cyclic voltammetry, and increased the capacitive performance [155], which was related to the large surface areas of TiO_2 nanorods, higher

amounts of water in RuO_2 structure. The optimum CV range was reported to be 0.25 to 1.45 V *vs*. Ag/AgCl.

Park *et al.* [156] deposited nano-crystalline and porous RuO_2 films on titanium substrates using a simple CED method, and a specific capacitance of 788 F g^{-1} was obtained, which was comparable with the *Cs* values achieved through other methods for the preparation of RuO_2 films. $RuO_2 \cdot nH_2O$ electrodes were deposited on Ti substrates by Zheng *et al.* [157], which showed a specific capacitance of 786 F g^{-1} with a deposit mass of 0.17 mg. The co-axial nanostructured RuO_x thin films were also electrodeposited onto the surface of the vertical graphitic nanofibers (GNFs), and excellent charge storage properties were observed for the fabricated RuO_x/GNFs/FTO electrode as compared with RuO_x/FTO and GNFs/FTO electrodes (Fig. 10) [158], which was attributed to the unique macro-porous structure and the coaxial nanostructure of RuO_x/GNFs films. It was also mentioned that GNFs play an attractive template for electrodeposited RuO_x film, and hence provide a large surface area and a facile charge transport pathway.

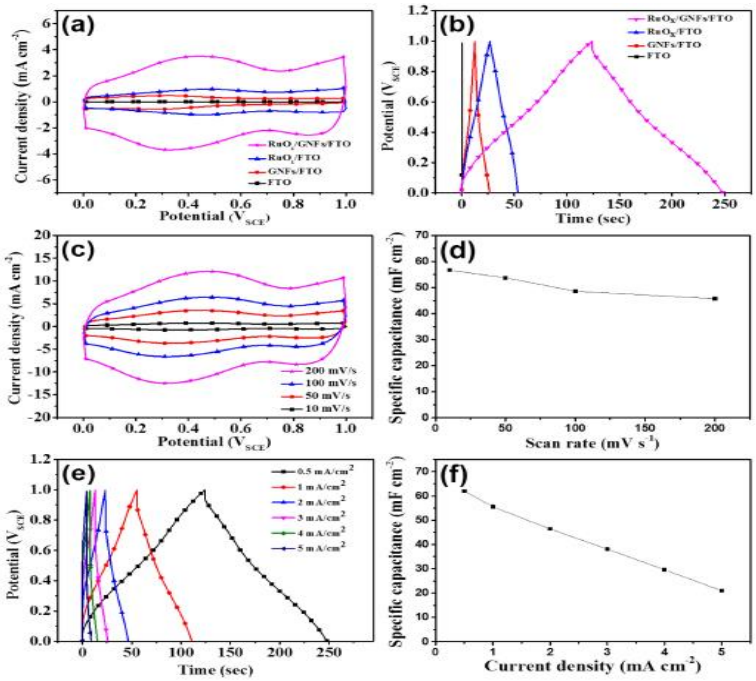

Fig. 10. (a) The CV curves of FTO, GNF/FTO, RuO_x/FTO, and RuO_x/GNFs performed at a scan rate of 50 mV s^{-1}; (b) The CD curves of FTO, GNFs/FTO, RuO_x/FTO, and RuO_x/GNFs/FTO performed at a current density of 1 mA cm^{-2}; (c) The CV curves of RuO_x/GNFs/FTO performed at the scan rates from 10 to 200 mV s^{-1}; (d) Calculated specific capacitance values at the scan rates from10 to 200 mV s^{-1}; (e) The CD curves of RuO_x/GNFs/FTO performed at the current densities from 0.5 to 5mA cm^{-2}; (f) Calculated specific capacitance values at the current densities from 0.5 to 5 mA cm^{-2}; (Reprinted with permission from Ref. [158], Copyright (2017) Elsevier)

Arunachalam *et al.* [159] developed a pulsed CED technique for fabricating a thin film $RuO_2 \cdot nH_2O$ onto Ni-flashed AISI 317 stainless steel (SS) substrate, and the specific capacitance of 520 F g^{-1} at the scan rate of 1 mV s^{-1} was observed. Porous RuO_2 was electrochemically decorated onto vertically aligned carbon nano-walls (CNW), and the prepared RuO_2/CNW electrode delivered a *Cs* of 1000 mF cm^{-2} (which was three orders of magnitude higher than state-of-the-art micro-supercapacitors), and the energy density comparable to that of Li-ion micro-batteries, yet with superior power and cycling stability [160]. Hydrous RuO_xH_y film with particle sizes of 5 nm and fine pore sizes of ~3–4 nm were also deposited from $RuCl_3$ bath using SBA-15 template [161]. A *Cs* value of 954 F g^{-1} and a high energy density of 32.7Wh kg^{-1} were obtained for the prepared material. Cho *et al.* [162] deposited RuO_2 onto a graphene (Gr)-coated Copper (Cu) foil by CED. The prepared flexible RuO_2/Gr/Cu electrode exhibited a specific capacitance of 1561 F g^{-1} (0.015 F cm^{-1}) at 5 mV s^{-1}, an improved retention of 98% under the bent condition, and an energy density of 13 Wh kg^{-1} at a power density of 21 kW kg^{-1}. The excellent capacitive capability of the prepared flexible RuO_2/Gr/Cu electrode was dedicated to the improved mechanical adhesion between ruthenium oxide film and the current collector.

2.2.2. Cobalt oxide

Among the various oxides candidate for use in supercapacitors, cobalt oxides (especially Co_3O_4) have been reported as the most proper ones due to their fast redox reactions and high theoretical specific capacitance (*Cs*=3560 F g^{-1}) [163-165]. Co_3O_4 undergoes Faradic charge storage mechanisms as a result of the following reactions [166]:

$$Co_3O_4 + OH^- \rightleftharpoons CoOOH + e^- \quad (11)$$

$$CoOOH + OH^- \rightleftharpoons CoO_2 + H_2O + e^- \quad (12)$$

To achieve better electrochemical performance, various Co_3O_4 nanostructures including nanorods [167,168], nanoparticles [169,170], nanowires [171], nano-flowers [172] etc., have been successfully prepared using different fabrication methods. In this regards, cathodic electrochemical deposition (CED) followed by heat-treatment (HT) has been applied as a versatile technique for the preparation of nano-scale cobalt oxides. For example CED, as a simple technique, was introduced by our group [173] for fabricating Co_3O_4 nanoplates. In this procedure, beta-$Co(OH)_2$ nanoplates were firstly deposited *via* constant current (CC) CED, and then HT was performed on the beta-$Co(OH)_2$ precursor at 500 ^oC for 3h to achieve oxide nanoplates, as schematically presented in Fig. 11 (provided from Ref. [173]). The fabricated nanoplates showed good capacitive performance including *Cs* value of 485 F g^{-1}, and 84.1% capacity retention after 3000 cycling at 5 A g^{-1}, which was attributed to the porous plate texture, and its high surface area [173].

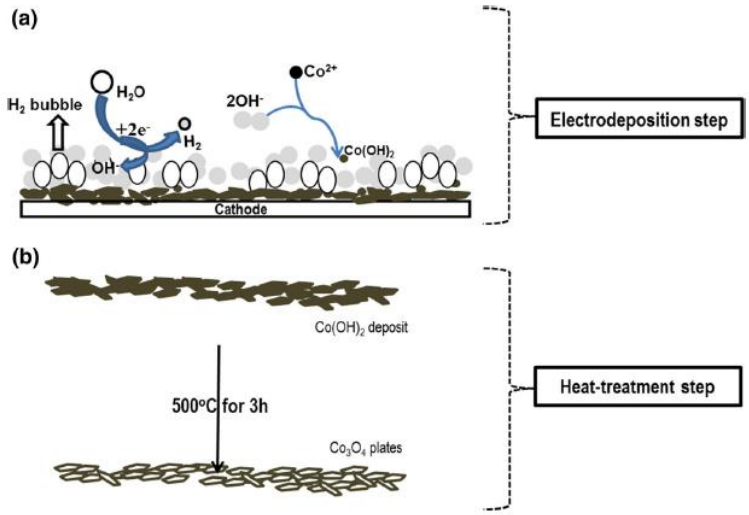

Fig. 11. Schematic view of Co_3O_4 preparation by electrodeposition-heat treatment step. (Reprinted with permission from Ref. [173], Copyright 2016 Springer)

A hierarchically porous Co_3O_4 film was also fabricated *via* CED using a liquid crystalline template by Yuan *et al*. [174]. The prepared film had a net-like structure of interconnected nano-flakes with a thickness of 15–20 nm, and a *Cs* value of 443 F g^{-1} (at 2 A g^{-1}) and 334 F g^{-1}(at 40 A g^{-1}), which was explained based on the unique hierarchically porous morphology of deposited oxide film. The effect of different modes of electrodeposition such as PD (potentiodynamic), PS (potentiostatic) and GS (galvanostatic) on the deposition of cobalt oxide and its supercapacitive performance were studied by Jagadale *et al.* [175].

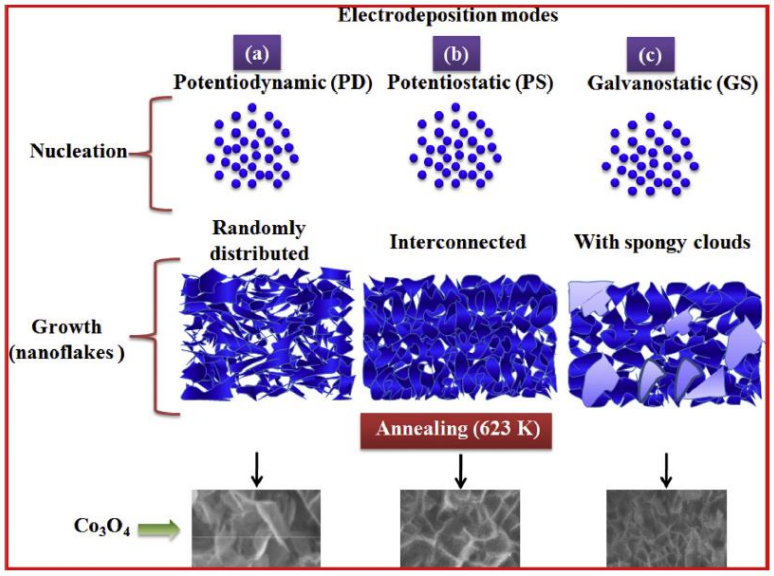

Fig. 12. Schematic representation of the formation of Co_3O_4 nanoflakes by (a) potentiodynamic, (b) potentiostatic and (c) galvanostatic modes of electrodeposition. Reprinted with permission from Ref. [175]. Copyright (2014) Elsevier)

The cobalt oxide film deposited under PS mode showed a maximum *Cs* value of 248 F g^{-1}, a specific energy of 2.3 Wh kg^{-1} and a specific power of 3.5 kW kg^{-1}, as compared with the samples obtained using GS and PD modes. The authors proposed the following schematic for the formation of the nanostructured oxide products (Fig. 12, provided from ref. [175]).

Capsule-like Co_3O_4 nanostructures were prepared *via* pulse CED followed by HT procedure [176]. The nanostructure delivered a high *Cs* value of 454.7 F g^{-1} (2 A g^{-1}) and a 94.5% *Cs* stability after 500 cycles. Furthermore, Wu *et al.* [177] reported porous Co_3O_4 a nano-walls/Ni and dense Co_3O_4 film/Ni foams prepared by CED [177], and observed *Cs* values of 325 F g^{-1} (at 2 A g^{-1}) and 247 F g^{-1} (at 40 A g^{-1}) for the nano-wall/Ni foam, which was much higher than that of the dense oxide film/Ni foam (i.e. *Cs*=230 F g^{-1} at 2 A g^{-1} and *Cs*=167 F g^{-1} at 40 A g^{-1}). They assigned the better PC capability of the porous Co_3O_4 nano-walls to its highly porous morphology, which originates the large surface area (SA) of Faradic reactions and short ion diffusion paths. Kung *et al.* [178] fabricated Co_3O_4 nanosheets/flexible Ti substrate through a one-step potentiostatic CED method followed by UV-ozone treatment for 30 min. For the fabricated electrode, the high *Cs* of 1033.3 F g^{-1} was obtained at 2.5 A g^{-1}. Using pulsed CED followed by HT, our group prepared high surface area Co_3O_4 nanosheets (SA=164 m^2 g^{-1}), and *Cs* value of 501.6 F g^{-1} at 2 Ag^{-1} and 89.9% *Cs* after 2000 cycles were observed for the prepared nanosheets (Fig. 13) [179].

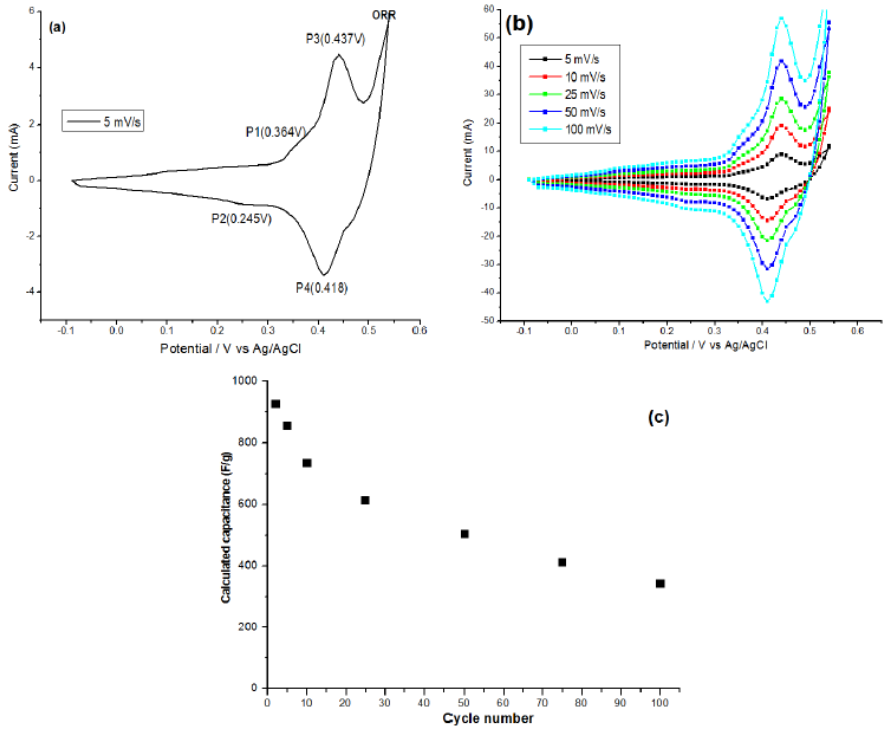

Fig. 13. (a) CVs of Co_3O_4 electrode at 5 mV s^{-1} and (b) at the various scan rates; (c) the calculated Cs values *vs*. scan rate. Reprinted with permission from Ref. [179]. Copyright (2016) ESG Publication

CED was also applied as simple one-step route for fabricating cobalt oxide composite electrodes. For example, Kim *et al.* [180] reported the on-step direct and uniform cathodic deposition of GO/Co_3O_4 thin films onto stainless steel substrate (SS). Before the cathodic deposition, GO was treated with PEI polymer, which acts as a stabilizer and linker between GO and Co^{3+} cations [180]. Galvanostatic cathodic electrodeposition of cobalt hydroxide was performed in an additive free nitrate bath at 60 ^oC, and then the resulting deposit was heat-treated at 400 ^oC for 3h [181]. The resulting powder exhibited an average pore diameter of 4.75 nm and the surface area of 208.5 $m^2\ g^{-1}$, which gave rise to the high capacitance of 393.6 F g^{-1} at 1 A g^{-1}.

García-Gómez *et al.* [182] prepared electrochemically rGO/cobalt oxide composites *via* two-steps of pulsed CED of hydroxide precursor onto SS electrode followed by calcination at 200 ^oC. The fabricated rGO/Co_3O_4/SS electrodes exhibited *Cs*=430 F g^{-1} at 1 A g^{-1} and good long-term cycling stability. Also, porous Co_3O_4 nanoplates with high surface area (SA=180 $m^2\ g^{-1}$) were made through pulsed-CED followed by heat-treatment [183], and the *Cs*420.5 F g^{-1} at a discharge load of 5 A g^{-1} has achieved. Zhang *et al.* [184] fabricated Co_3O_4@$Ni(OH)_2$ core/shell nanowire arrays (NAs) using CED and the Co_3O_4@$Ni(OH)_2$//AC asymmetric supercapacitor provided high specific energy (49.8 Wh kg^{-1} at 801 W kg^{-1}) and specific power (16.1 kW kg^{-1} at 28.1 Wh kg^{-1}). Moreover, Pavul Raja *et al.* [185] demonstrated the single CED synthesis of a cobalt oxide–polyindole composite through *in-situ* CED [185], and the specific capacitance of polyindole decorated electrode was found to be 1805 F g^{-1} at 2 A g^{-1}. Further an excellent rate capability (*Cs*=1625 F g^{-1} at high discharge load of 25 A g^{-1}) was also observed, due to the synergism evolved between Co_3O_4 and Polyindole.

Rakhi *et al.* [186] constructed a directly-grown composite electrode through the cathodic electrodeposition of nanocrystalline, hydrous RuO_2 NPs dispersed on the CED produced mesoporous Co_3O_4 nanosheets, and observed an excellent specific capacitance of 905 F g^{-1} (at current load of 1 A g^{-1}) and a 78% constant rate GCD cycling performance at current load ranging from 1 to 40 A g^{-1} [186]. Jagadale *et al.* [187] potentio-dynamically deposited cobalt hydroxide from a cobalt chloride electrolyte and then calcined the product at 350 ^oC for 3h to produce Co_3O_4 nanoflakes on a stainless steel substrate. They reported *Cs*=365 F g^{-1}, energy and power densities of 64 Wh kg^{-1}, and 21.53 kW kg^{-1}, as well as a 99% coulombic efficiency for the CED fabricated electrode. The composite ERGO/CoO_x@SS electrode was also prepared through cyclic voltammetric deposition onto a stainless steel substrate using a mixed graphene oxide and cobalt nitrate electrolyte [188]. The optimal deposition scan rate, number of cycles, and concentration ratio of GO/$Co(NO_3)_2$ in the deposition bath were reported to be 75 mV s^{-1}, 25 cycles, and 0.5/0.5 mg ml^{-1}, respectively. The fabricated electrode at these optimum parameters exhibited a *Cs* of 608 F g^{-1} at 1 A g^{-1}. Kazazi *et al.* [189] used cathodic electrophoretic deposition followed by galvanostatic cathodic electrochemical deposition (i.e. EPD-CED) to fabricate a binder-free Co_3O_4-CNTs pseudo-capacitive electrode.

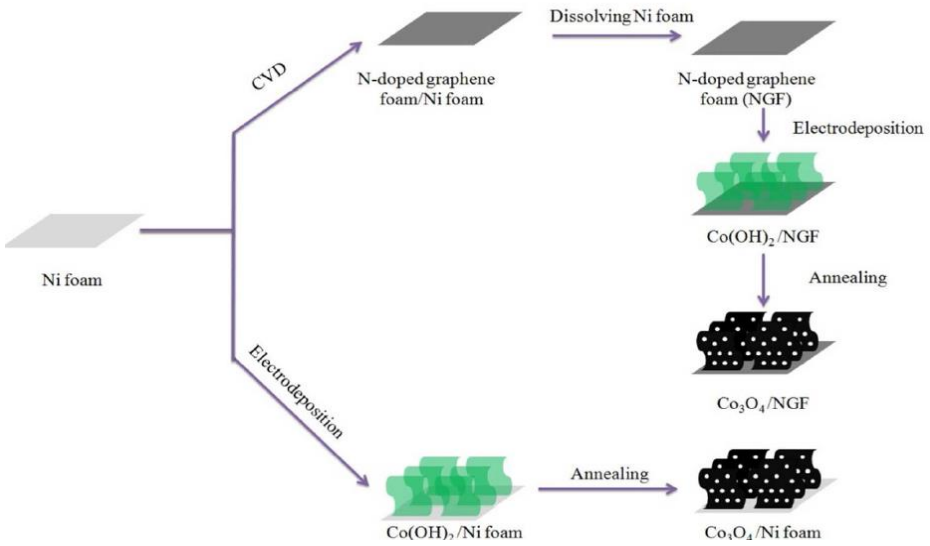

Fig. 14. Schematic depiction of the synthesis of Co_3O_4/NGF and Co_3O_4/Ni foam. (Reprinted with permission from Ref. [192], Copyright (2015) American Chemical Society)

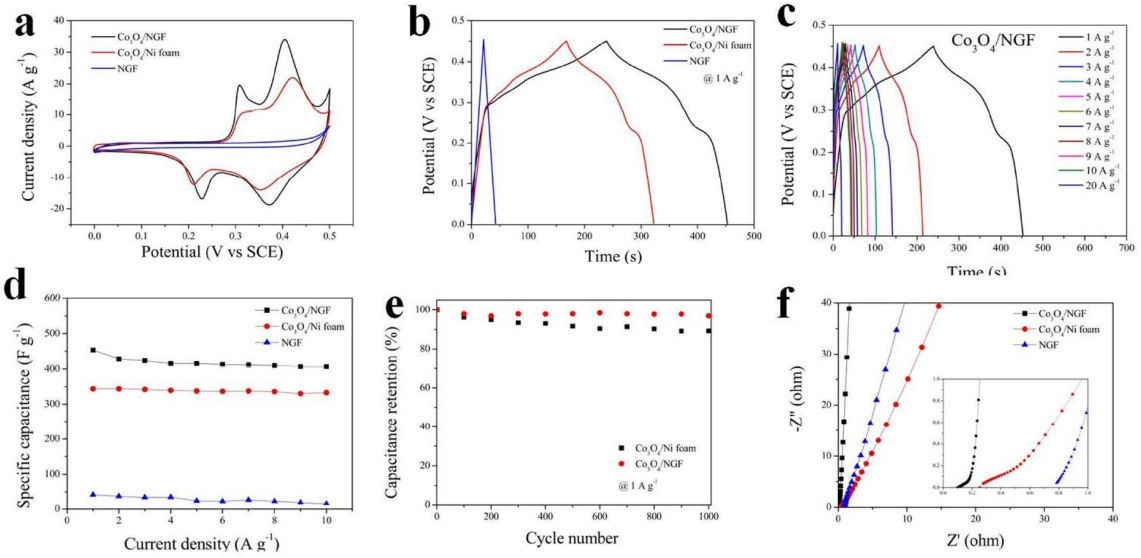

Fig. 15. Electrochemical performance of NGF, Co_3O_4/Ni foam and Co_3O_4/NGF composite using three electrode cell in 1 M KOH. (a) CVs of as-prepared samples at the scan rate of 20 mV s^{-1}; (b) Galvanostatic charge/discharge curves of as-prepared samples at discharge current density of 1 A g^{-1}; (c) Galvanostatic charge/discharge curves of Co_3O_4/NGF at different current densities; (d) Specific capacitance of as-prepared samples at different discharge current densities; (e) Cycle performance of as-prepared samples at discharge current density of 1 A g^{-1}; (f) Nyquist plots of as-prepared samples (0.01 Hz to 100 KHz, with an AC amplitude of 5 mV. (Reprinted with permission from Ref. [192], Copyright (2015) American Chemical Society)

They deposited CNTs on the surface of a chemically activated graphite sheet by EPD from ethanolic suspensions and then electrodeposited a cobalt oxide thin film onto the CNT-coated graphite substrate through a galvanostatic CED method followed by HT. The prepared electrode offered a high areal capacitance of 4.96 F cm^{-2} (at 2 mA cm^{-2}) and a 91.8% cycling stability after 2000 cycles, which was attributed to the superior electrical conductivity of CNTs and the porous oxide structure with high surface area (144.9 m^2 g^{-1}).

Cathodically growing a hydroxide precursor onto cobalt substrate at RT, followed by subsequent heat-treatment, freestanding Co_3O_4 nanosheets with 2D hexagons morphology have also been synthesized [190].

Yuan *et al.* [191] fabricated ultrathin mesoporous Co_3O_4 nano-sheet arrays onto Ni foam by CED, and the superior pseudo-capacitive performance of 2735 F g^{-1} was observed. Recently, two types of Co_3O_4/Ni foam and Co_3O_4/NG foam have been fabricated using potentiostatic CED followed by HT (Fig. 14) [192]. The Co_3O_4/NG foam was composed of mesoporous nanosheet on nitrogen-doped graphene foam (NGF), and exhibited high *Cs* ability (i.e. 451 F g^{-1}) as compared with those of NGF and Co_3O_4/Ni foam (Fig. 15). The enhancement was attributed to the unique 3D hierarchical electrode structure, mesoporous nanosheets with pore sizes of 3-8 nm and the synergistic effect of Co_3O_4 and NGF [192].

2.2.3. Iron Oxides

Generally, iron oxide has different crystallographic forms of, FeO (wustite), α-Fe_2O_3 (Hematite), γ-Fe_2O_3 (Maghemite) and Fe_3O_4 (Magnetite), depending on the atomic arrangements of iron(III) cations and oxygen anions [193]. These oxides constitute promising materials for use in SCs as a result of their natural abundance, low cost, variable oxidation states, and high theoretical capacitances [194]. The capacitance of hematite in a sodium sulfite electrolyte results from the faradic reactions between iron(II) and iron(III) cations together the SO_3^{2-} ions intercalation [194]. The charge storage ability of magnetite-based electrodes has been studied by Wu *et al.* [195]. They investigated the *Cs* values delivered by magnetite in various aqueous electrolytes of 1M Na_2SO_3, saturated Na_3PO_4, 1 M Na_2SO_4, 1 M NaCl and 1 M KOH [195], and found that Fe_3O_4 electrodes (in an Na_2SO_3 electrolyte) deliver a very high *Cs* value of 510 F g^{-1} as compared with those observed in other electrolytes. Also, the combination of both EDLC and PCs was observed for Fe_3O_4 in an Na_2SO_3 electrolyte [195,196]:

$$2SO_3^{2-} + 3H_2O + 4e^- \leftrightarrow S_2O_3^{2-} + 6\ OH^- \quad (13)$$

$$S_2O_3^{2-} + 3H_2O + 8e^- \leftrightarrow 2S^{2-} + 6\ OH^- \quad (14)$$

In this section, the publications on the CED preparation of magnetite- and hematite-based electro-active materials for SC applications have been reviewed. Notably, CED method has

been extensively applied for the preparation of pure and doped Fe_3O_4 electrodes, where there are only few reports on the cathodic electrodeposition of Fe_2O_3 nanomaterials [197]. For example, ultra-fine nanoparticles (NPs) of magnetite iron oxide (Fe_3O_4) were prepared through PVA-assisted cathodic electro-synthesis, from a bath containing 0.005 M $Fe(NO_3)_3$, $FeCl_2$ and 0.1 g/L PVA [198], and specific capacitance of as high as 195.8 F g^{-1} at 0.5 A g^{-1} and 94% *Cs* retention after 3000 cycles were observed. Zn^{2+}-doped Fe_3O_4 NPs were prepared *via* a one-pot CED method from a mixed $Fe(NO_3)_3/FeCl_2/ZnCl_2$ (0.005VM) electrolyte and a *Cs* value of 164.3 F g^{-1} at 1 A g^{-1}, and 89.4% capacity retention after 1000 GCD cycling were delivered by Zn- Fe_3O_4 electrode (Fig. 16) [199].

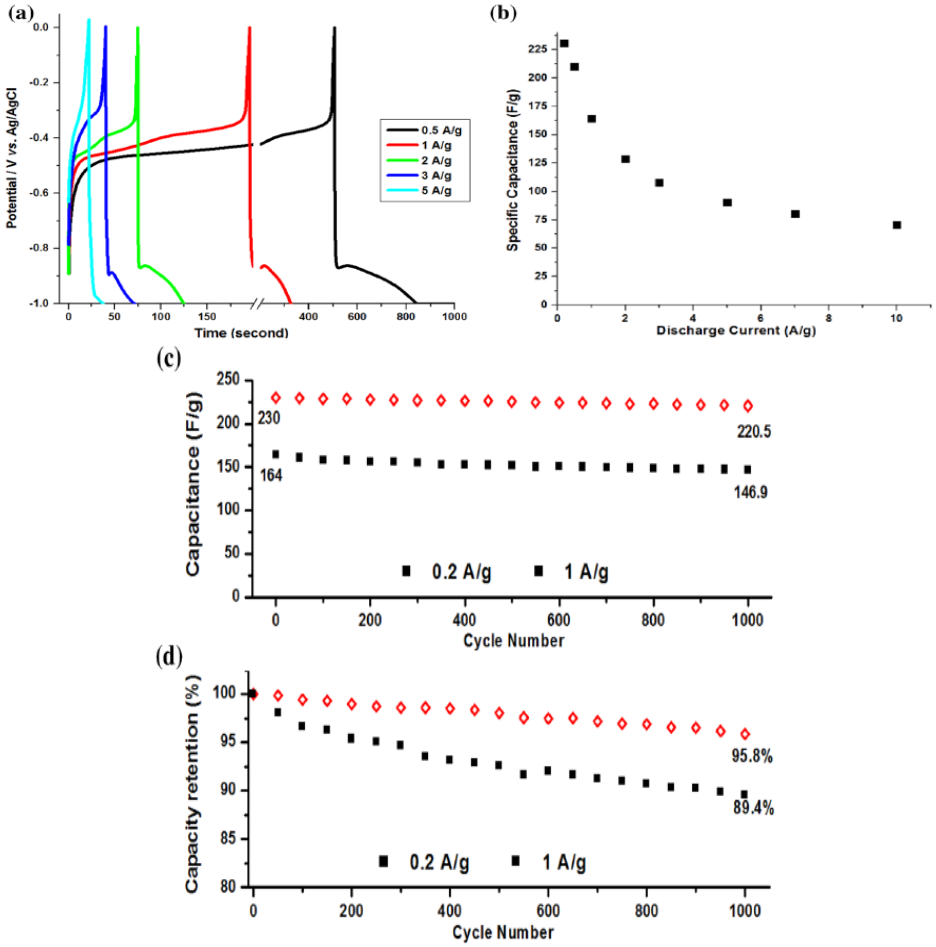

Fig. 16. (a) GCD profiles of Zn- Fe_3O_4 electrode and (b) is calculated SCs at the different current loads of 0.5 to 5 A g^{-1}; (c) capacity values and (d) capacity retention for 1000 GCD cycling at 0.2 and 1 A g^{-1}. (Reprinted with permission from Ref. [199], Copyright 2017 Springer)

A Dy^{3+}-doped Fe_3O_4 nano-electrode was also fabricated through a one-pot CED platform using an aqueous mixed solution of Fe(III) nitrate, Fe(II) chloride and Dy(III) chloride salts as

the electrolyte, and Dy^{3+}-doped Fe_3O_4 electrode showed a *Cs* value of 202 F g^{-1} at 0.5 A g^{-1}, and 93.9% capacity retention after 2000 cycles [200]. Furthermore, an Eu^{3+}-doped Fe_3O_4 nano-electrode was fabricated in the same way from an $Fe(NO_3)_3/FeCl_2/EuCl_3$ electrolyte, and a *Cs* of 212.5 F g^{-1} was reported at 0.5 A g^{-1} [201]. Through a one-step CED process, undoped and (15% wt.) La^{3+}-doped Fe_3O_4 nanoparticles were prepared [202]. The doped electrode exhibited *Cs* a value of 187 F g^{-1} and an 84.8% *Cs* retention after 2000 discharging cycles at 1 A g^{-1}, which was 20% greater than those of the un-doped electrode (i.e. *Cs*=145 F g^{-1} and cycle life=78.7%). Furthermore, 15-20% capacity improvement was reported for magnetite electrodes doped with Cu^{2+} [203] and Sm^{3+} [204]. Notably, the same results were also observed by our group for manganese-, nickel- and praseodymium-doped iron oxide NPs [205-207]. For example, Cs values as high as 221, 194, 171, 139, 112, 94 and 82 F g^{-1} were delivered by Pr-doped electrode at the potential sweeps of 2, 5, 10, 20, 50, 75 and 100 mV s^{-1}, which were~20% greater than those of un-doped electrodes with *Cs* values of 181, 159, 140, 112, 92, 83 and 68 F g^{-1} at the potential sweeps of 2, 5, 10, 20, 50 and 100 mV s^{-1}, respectively [206]. Nickel-doped nano-electrode exhibited *Cs* values of 228.2 F g^{-1} (at 0.25 A g^{-1}), 194.4 F g^{-1} (at 0.5 A g^{-1}), 168.8 F g^{-1} (at 1 A g^{-1}), 137 F g^{-1} (at 2 A g^{-1}), and 61.4 F g^{-1} (at 10 A g^{-1}), and a 15% enhancement in SC performance of Fe_3O_4-based electrode (Fig. 17) [207].

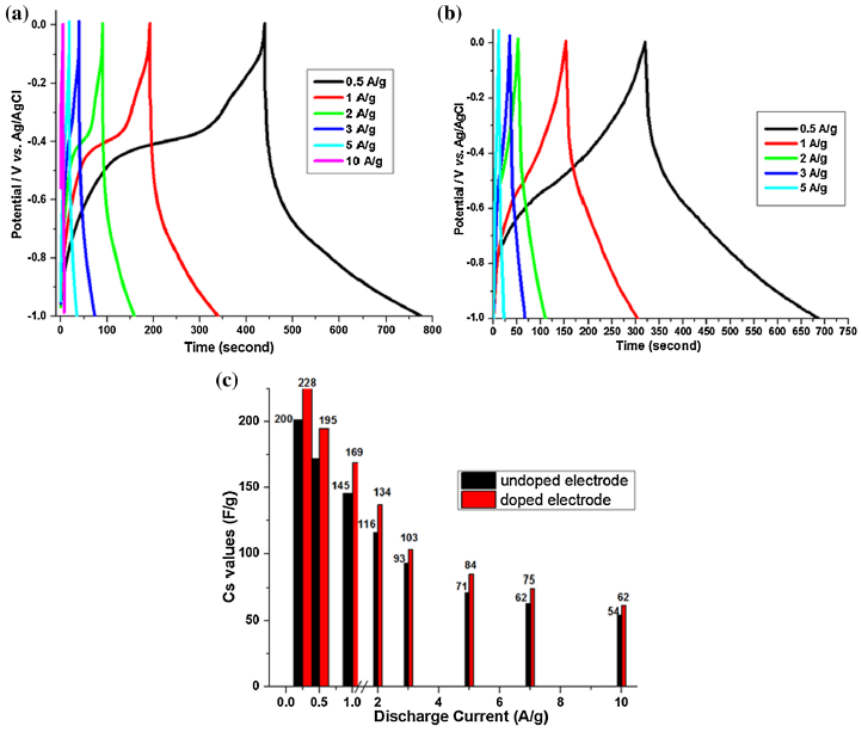

Fig. 17. GCD profiles of the fabricated (a) Ni-doped and (b) undoped electrodes and (c) their calculated *Cs* values at the different current loads of 0.2 to10 A g^{-1}. (Reprinted with permission from Ref. [206]. Copyright 2018 Springer)

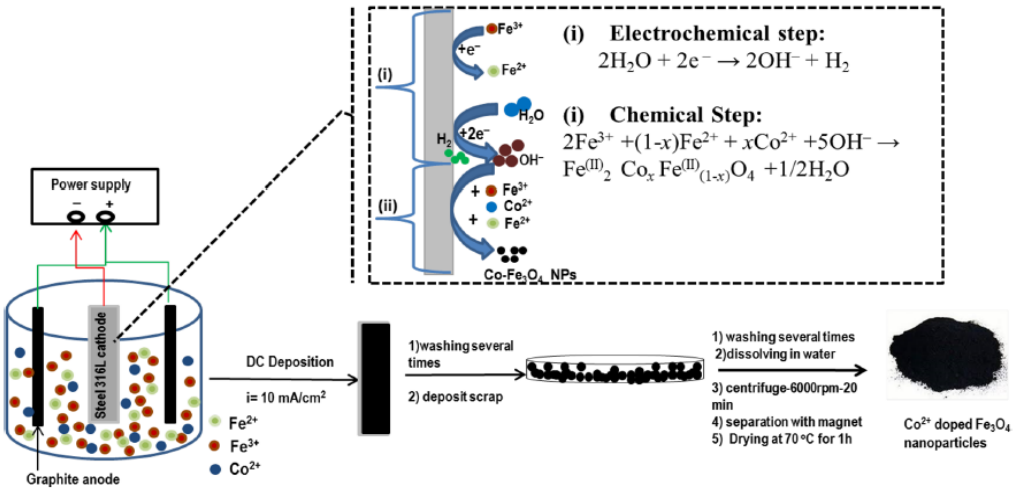

Fig. 18. Schematic graph of the cathodic electrodeposition of Co^{2+} doped IONPs. The inset provides deposition mechanism; i.e. (i) electrochemical and (ii) chemical steps. (Reprinted with permission from Ref. [211], Copyright (2017) Elsevier)

Very recently, we reported Gd^{3+}- and Bi^{3+}-doped magnetite electrodes prepared through CED, and these electrodes exhibited *Cs* values of 190.1 F g^{-1} and 171 F g^{-1} at 0.5A g^{-1}, respectively [208,209]. Furthermore, using a one-pot CED synthesis, holmium- and cobalt-doped iron oxide nanoparticles were simply synthesized by our group, and the fabricated electrodes showed about 20% higher Cs values as compared with the un-doped electrode [210,211], which was assigned to the pure magnetite phase, fine size (~5 nm) and high surface area (~150 m^2/g). The schematic presentation of the cobalt doping of the magnetite NPs can be seen in Fig. 18 [211]. Our group found that the supercapacitive performance of iron oxide electrodes could be enhanced though the fabrication of ultra-fine, well-dispersed particles through a PEG-assisted CED route [212].

10wt% yttrium-doped 20nm Fe_3O_4 nanoparticles were produced through CED, and showed a *Cs* of 190.3 (at 0.25 A g^{-1}) and 138.9 F g^{-1} (at 1 A g^{-1}), and *Cs* stabilities of 95.9% and 88.5% after 2000 GCD cycling [213]. Similar results have been reported for cathodically deposited cadmium-, aluminum- and cerium-doped iron oxide electrodes [214-216]. Lokhande *et al.* [217] showed that the supercapacitive performance of Fe_2O_3 electrode is completely dependent on the OH^- concentration. Fabrication of γ-Fe_2O_3 films were performed through CED by Nagarajan and Zhitomirsky [218], and the capacitive abilities of the deposited films were studied in 0.25 M Na_2SO_4 and 0.25 M $Na_2S_2O_3$ electrolytes. They found that a higher Cs value of 210 F g^{-1} could be achieved in $Na_2S_2O_3$ electrolyte, and the observed that charge storage performance of γ-Fe_2O_3 decreased with increasing the film thickness, while it was increased by heat-treatment at 140°C. Mitra *et al.* [219] reported that preparation of Fe_3O_4 deposits with various morphologies could be achieved by manipulating the deposition time and the bath temperature, where thick films with well-faceted particles of Fe_3O_4 could be obtained at long deposition times, and thin and shapeless deposits were formed after short deposition times.

Chung *et al.* [220] deposited a pure, high crystalline nano-sized cellular Fe_3O_4 thin film, on Pt and the resulting electrode showed 105 F g^{-1} in 1 M Na_2SO_4. Using CED/HT process, PEDOT@MnO_2 and C@Fe_3O_4 composites were formed and used as positive and negative electrodes, respectively. The fabricated fiber-shaped supercapacitor showed a wide working potential window (2 V), high areal *Cs* of 60 mF cm^{-2} and large energy density of 0.0335 mWh cm^{-2} [221].

2.2.4. Nickel oxide

Nickel oxide (NiO) is especially attractive as the electro-active material for SC applications because of its high theoretical capacitance of 2573 F g^{-1} [222], environment friendliness, and good thermal and chemical stability [223]. Due to fast redox reactions, shortened diffusion paths and high specific surface areas in the solid phase, NiO micro/nanomaterials were investigated for electrochemical capacitors (ECs) [224,225]. Hence, NiO nanostructures including nano-porous films, NPs, NWs, nano-flowers, and hollow nano-fibers were prepared by different chemical methods (i.e. hydrothermal, solvothermal, precipitation, thermal decomposition) and investigated as electrode materials in SCs [226]. For instance, cathodic electrochemical deposition followed by heat-treatment (CED-HT) has been also mentioned as a facile procedure for synthesis of various nanostructures of this oxide material. Accordingly, nano-capsules of NiO were synthesized through HT of the CED prepared $Ni(OH)_2$ at 300 °C for 3h [227], where the capacitive performance of the NPs prepared *via* CV and GCD had *Cs* values, as high as 307.2 F g^{-1} in 1 M KOH solution and an 86.4% retention after 3000 cycles (as seen Fig. 19, which provided from Ref. [227]).

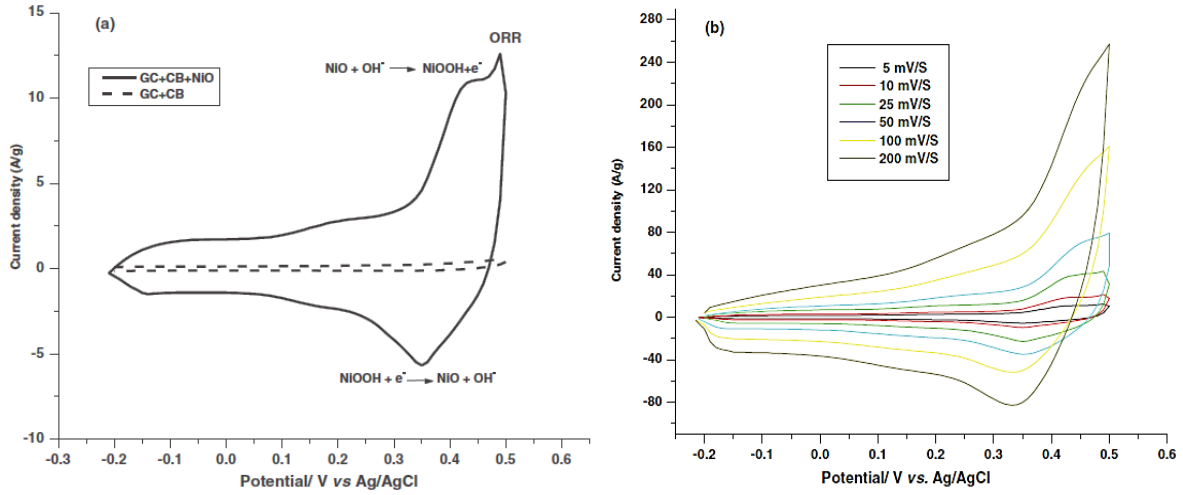

Fig. 19. Cyclic voltammogram of (a) NiO nanocapsules compared with blank electrode and (b) its CVs at various scan rates. GC: Glassy carbon and CB: Carbon black. (Reproduced with permission from [227], Copyright 2012, The Electrochemical Society)

The following the mechanism has been proposed for NiO capacitive performance [227,228]:

(i) Formation of NiOH layer at the surface of the oxide electrode:

$$NiO + H_2O \rightarrow Ni(OH)_2 \text{ (at the oxide surface)} \quad (15)$$

(ii) Charge transfer based on surface Faradaic Ni^{2+}/Ni^{3+} redox reaction in a basic electrolyte:

$$Ni(OH)_2 + OH^- \rightarrow NiOOH + H_2O + e^- \quad (16)$$

Crystalline cubic NiO nanoplates was also fabricated using a galvanostatic CED-HT process, and for the fabricated electrode, had a *Cs* of 481.16 Fg^{-1}, a specific power of 19.48 kW kg^{-1}, a specific energy of 60.12 Wh kg^{-1} and a 92.31%, Coulombic efficiency [229]. Our group has also fabricated NiO nanoplates through the CED-HT approach as illustrated in Fig. 20 [230], and the nanoplates exhibited good reversibility (i.e. ΔE_p=22 mV), proper Cs (1345 F g^{-1}) and 89.1% long-term cycling stability after 3000 at load of 1 A g^{-1}. The formation mechanism is given in Fig. 21 from Ref. [230].

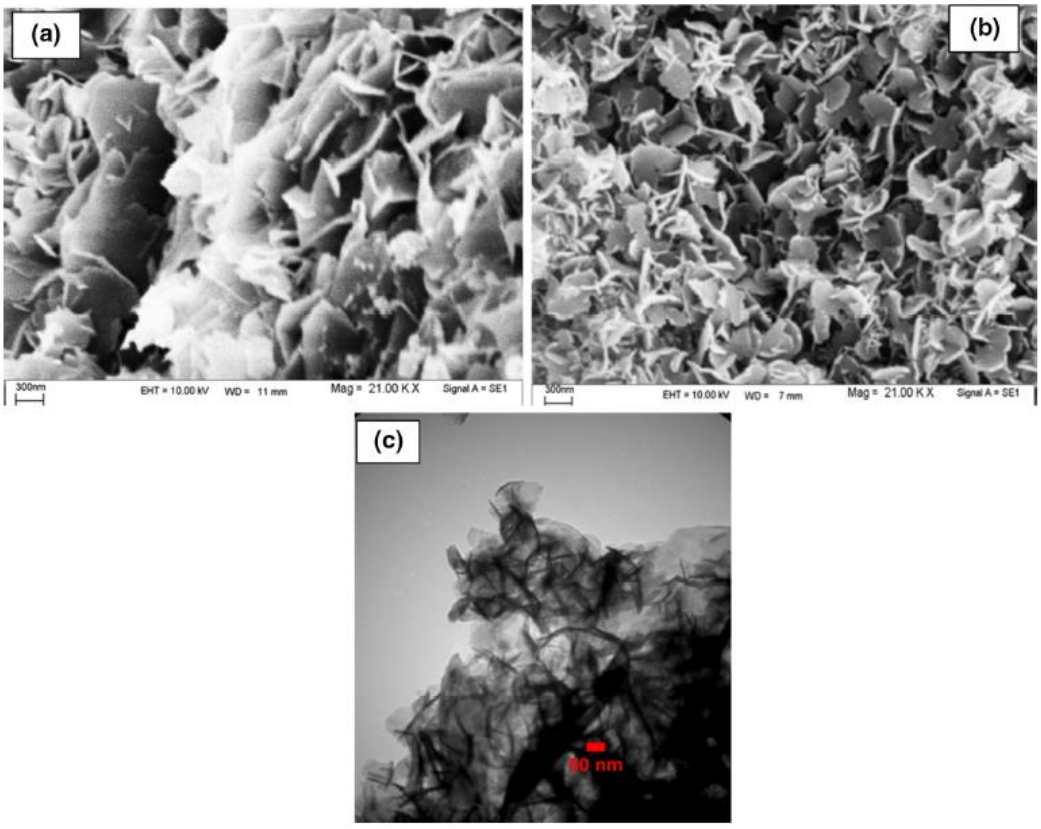

Fig. 20. SEM image of (a) electrodeposited precursor; (b) SEM and (c) TEM images of final oxide sample. (Reprinted with permission from Ref. [230], Copyright 2017 Springer)

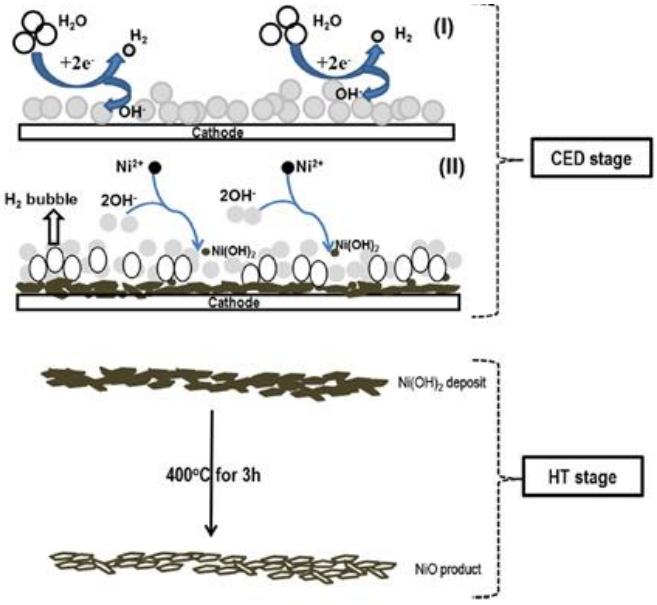

Fig. 21. Schematic view of NiO preparation by cathodic electrochemical deposition-heat treatment (CED-HT) method. (Reprinted with permission from Ref. [230]. Copyright 2017 Springer)

Zeng *et al.* [231] applied potentiostatic CED followed by HT for preparing the Co_3O_4-NiO nano-flowers onto Ni foam, and a Cs of 687.5 F g^{-1} (0.5 A g^{-1}) and a 94% cycling stability after 2500 cycles were reported. Also, Die *et al.* [232] used CED as a novel template-free electrochemical approach for fabricating an $Ni(OH)_2$/NiO/Ni composite also containing a nanotube array films on Ni foam, which delivered a *Cs* of 1070 F g^{-1} at 15 A g^{-1} after 10000 cycles. Edison *et al.* [233] used an electrochemically designed Ni foam to form NiO_x NPs/Ni foam by CED/HT of $Ni(OH)_2$ and obtained a capacitance of 60.7mAh/g at 5 mV/s. Barani *et al.* [234] reported well-dispersed NiO-NPs prepared by constant current CED followed by heat-treatment, where nanoparticles provide high *Cs* of 1623.1 Fg^{-1} at 5 mVs^{-1} and 93.4% capacity decay after 1000 cycling at 2 A g^{-1}. This was attributed to the fine size and high surface of the fabricated oxide particles. Electrochemically deposited 3D graphene/NiO onto Ni foam were developed by Shahrokhian *et al.* [235], and a high specific capacitance of 1715.5 F g^{-1} at 2 A g^{-1} was delivered by ERGO-NiO@Ni foam electrode, which related to the hierarchical morphological structure facilitating the diffusion of the electrolyte into the electrode material. Furthermore, CED-based NiO electrode were reported to have a *Cs* of as high as 458 F g^{-1} at 5mV/s, a specific energy of 10.90 Wh kg^{-1}, a specific power of 0.89 kW kg^{-1}, and a 98% Coulombic efficiency [236]. A LaO_x-NiO@ Ni foam composite electrode was synthesized *via* CED followed by thermal annealing without any binders [237]. The electrode had a proper electrochemical performance (i.e. *Cs*= 1238 F g^{-1} at 0.5 A g^{-1}, and 93% *Cs* stability after 10000 cycles), which has been ascribed to the unique Ni/La layered structure and more redox sites provide by LaO_x particles. Through the potentiodynamic cathodic electrodeposition and

subsequently calcination at 473 K for 2h, Kumbhar *et al.* [238], prepared a NiO/nickel foam electrode, which composed of corn flake-like nanostructures. The electrode delivered a *Cs* of 1717 F g^{-1} and 87% capacitance retention after 5000 cycles. Furthermore, the high energy density of 44 W h kg^{-1} and the power density of 14 kW kg^{-1} were obtained for the constructed NiO//AC asymmetric supercapacitor using a polyvinyl alcohol-KOH gel electrolyte. The performances were considered as being the result of the highly porous texture of the NiO flakes [238].

Pulsed CED was also applied for preparing the NiO electrode. For example, our group fabricated NiO rods/plates through pulsed CED of $Ni(OH)_2$ followed by HT at 400 °C for 2h [239]. The material showed a *Cs* of 1445 F g^{-1} (at 1 A g^{-1}) and a 91.8% capacity retention after 3000 cycling. Also, a highly porous 3D NiO nanostructure was prepared *via* pulsed CED/HT at 500 °C for 3h, which led to a *Cs* value of 1056.4 F g^{-1} and a 89.7% capacity retention of after 3000 cycles at 3 A g^{-1} [240]. The deposition parameters were t_{on}=1s, t_{off}=1s, i_{peak}=50 mA cm^{-2}, T_{bath}=80 °C and $t_{deposition}$=30 min. The green hydroxide powder was then calcined at 500 °C for 3h to obtain a black oxide powder [240]. Uniform NiO NPs were prepared through potentiostatic CED of $Ni(OH)_2$ from 0.08 M $Ni(NO_3)_2$ onto a nickel foil at a potential of -0.90 V *vs*. SCE followed by HT at 250 °C for 2 h. The *Cs* value was 1478 F g^{-1}, and the material had excellent rate capability and long cycle ability [241].

Liu *et al.* [242] electrodeposited NiO nanosheets onto a 3D ultra-thin graphite film ((UGF)/CNT), and observed a *Cs* value of 575.6 F g^{-1} at 10 A g^{-1} and 100% *Cs* stability after 3000 cycles at 1 A g^{-1}. Zhang *et al.* [243] grew CNTs on a carbon fiber paper (CFP) through a CVD system, and then electrodeposited NiO NPs onto this flexible substrate through CED technique, and used the resulting assembly as a flexible electrode for SCs. The fabricated NiO@CNTs/CFP electrode displayed a *Cs* value of 1317 F g^{-1} at 1.2 A g^{-1}, as well as a 90.6% retention at 9.6 A g^{-1} 3000 cycles [243]. Su *et al.* [244] used a 0.1 M $NaNO_3$+1.0 M Ni $(NO_3)_2$+1.0 M $Co(NO3)_2$ solution as the electrolyte to deposit NiO and Co_3O_4 onto CNT yarn, and observed that the two-ply yarn supercapacitor based on the CNT@Co_3O_4 composite exhibited better electrochemical properties than supercapacitors based on pure CNT yarn and the CNT@NiO yarn.

2.2.5. Mn Oxides

Mn oxides (MnO_2, Mn_3O_4 and Mn_2O_3) are promising candidates as electrode material for electrochemical SCs due to their low cost and excellent capacitive performance in the aqueous electrolytes [245-247]. The charge storage mechanism of MnO_2 is ascribed to the following reaction [245]:

$$MnO_2 + B^+ + e^- \leftrightarrow MnO_2B \quad (17)$$

where B^+= Li^+, Na^+, K^+ and H^+.

From Eq. (17), it is revealed that large SAs, high ionic and electronic conductivity are needed to achieve high electrochemical performance of MnO_2 electrode and its high theoretical capacity (*Cs*=1380 F g^{-1}) [248,249]. MnO_2 has different crystal phases (i.e. α-, β-, γ-, δ- and λ-MnO_2), and it is mentioned that the tunnel size limits the cations intercalation and so determine MnO_2 charge storage performance [247,249]. Hence, many research studies have been performed to fabricate high surface area nano-structured MnO_2, which is completely dependent to the synthesis method [249]. In this regards, different nanostructures of manganese dioxides have been fabricated by CED. This part reviews some of these efforts. For example, an MnO_2–CNTs nanocomposite was fabricated by CED, and showed a *Cs* value of 356 F g^{-1} at 2 mV s^{-1} [250]. Mn_3O_4 and α-MnO_2 nanorods were also fabricated OH^- electrogeneration at a cathode in a two-electrode system, and their supercapacitive performance was also evaluated by CV and GCD tests [251,252]. α-MnO_2 nanorods had an energy storage ability of 338 F g^{-1} at10 mVs^{-1} [252]. Furthermore, MnO_2@NiAl LDH nanostructures with porous flower-like morphologies were formed on a Ni foam using a one-pot base generation strategy on the cathode [253]. The electrode exhibited enhanced charge storage properties (e.g. *Cs*=1554 F g^{-1} at 1 A g^{-1}) as opposed to pure MnO_2 (*Cs*=439 F g^{-1}) and NiAl-LDHs (*Cs*=742 F g^{-1}), which attributed to the close contact and proper MnO_2 dispersion on the NiAl-LDHs layer, and hence the synergy between the components of this two component of electrode. Nguyen *et al.* [254] reported the cathodic electrodeposition of MnO_2 films from a Mn nitrate electrolyte *via* a base generation strategy, and the deposited films showed the *Cs* value of 196 F g^{-1} after 1000 continuous GCD cycles at 1 A g^{-1}. Pulsed CED was used to form MnO_2 nano-worms using a 0.005 M $MnCl_2$ solution in the presence of CTAB Tizfahm *et al.* [255], and the *Cs* value of the fabricated working electrode was reduced from 239 F g^{-1} to 207 F g^{-1} after 1000 cycles at 2 A g^{-1}. The applied pulse CED parameters were reported to be t_{on}=1*ms*, t_{off}=1*ms* and I_a=10 mA cm^{-2}. Using pulse base OH^- electrogeneration (t_{on}=10 *ms* and t_{off}=50 *ms* and I_a=1 mA cm^{-2}), cathodic electrodeposition of Mn_3O_4 nanorods from Mn chloride was achieved [256]. The product had a specific capacitance of 321 F g^{-1} at 2 mV s^{-1}, and cycling stabilities of 91.7% (at 1 A g^{-1}), 83.4%(at 5 A g^{-1}), and 75.7% (at 10 A g^{-1}) after 1000 cycles. Hao *et al.* prepared Mn_3O_4 nanosheets by a simple galvanostatic cathodic electrodeposition in 0.1 M $MnSO_4$ solution, and then carried out the phosphatization of the prepared Mn_3O_4 nanosheets *via* cyclic voltammetry method in aqueous solution including 0.1 M $Na_3PO_4.12H_2O$ [257]. They used the synthesized phosphate ions manganese oxide (PMn) nanosheet arrays as binder-free electrode materials [257], and observed that *Cs* of the PMn electrode at 5 mV s^{-1} (*Cs*=6.7 mF cm^{-2}) was higher than that of the Mn_3O_4 electrode (*Cs*=2.7 mF cm^{-2}) and mentioned that the modification of Mn_3O_4 electrode with phosphate ions effectively prevents the Mn_3O_4 dissolution and results in a significant improvement. Yang *et al.* [258] reported coating vertically-aligned $Mn(OH)_2$ nano-sheet on a flexible Au coated polyethylene terephthalate substrate by CED. The electrochemical analyses by GCD revealed the *Cs* value to be as high as 240.2 F g^{-1} at 1 A g^{-1}

for this electrode, due to the vertically-aligned configuration of deposited nanostructure. Mn_3O_4 nanorods with secondary plate-like structures (Fig. 22) were prepared *via* direct current mode cathodic deposition from a 0.005M $MnCl_2$ bath [259], and *Cs* value of 298 F g^{-1}, and 95.1% cycling stability after 1000 cycles observed for nanorods (Fig. 23).

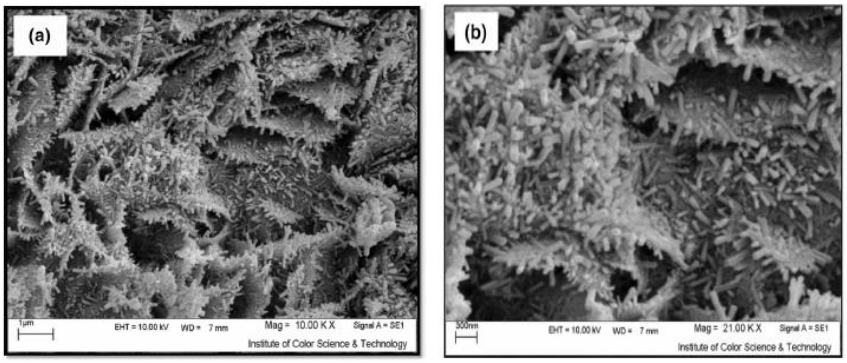

Fig. 22. SEM images of the prepared Mn_3O_4. (Reprinted with permission from Ref. [259]. Copyright 2016 Springer)

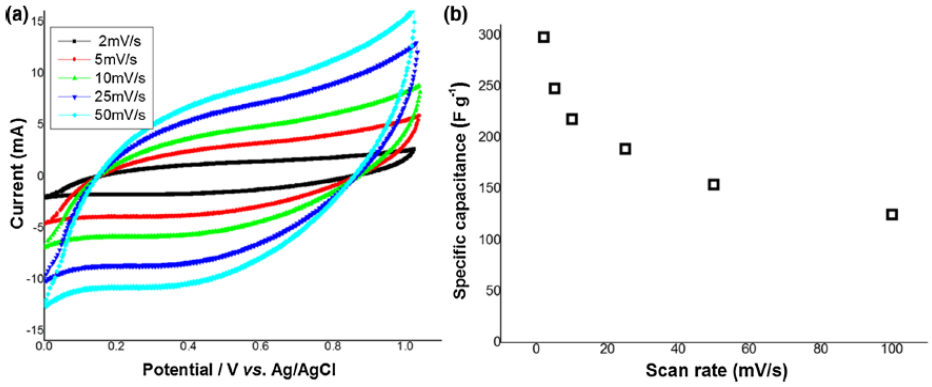

Fig. 23. (a) Cyclic voltammograms of the Mn_3O_4 electrode at various scan rates of 2, 5, 10, 25 and 50 mV s^{-1}; and (b) the calculated specific capacitances from CV curves. (Reprinted with permission from Ref. [259]. Copyright 2016 Springer)

An MnO_2-SiO_2 composite film was fabricated on a stainless steel substrate by CV deposition, and then removing the SiO_2 template by a simple immersion in concentrated basic media to produce a porous MnO_2 electrode [260]. Nguyen *et al.* [261] prepared micro/nano porous manganese oxide electrode through cathodic deposition onto stainless steel using dynamic hydrogen bubble templating (DHBT) [262], and observed a *Cs* value of 305 F g^{-1} at 1 A g^{-1}, and 61% rate capability at the current loads ranging from 1 A g^{-1} to 10 A g^{-1}.

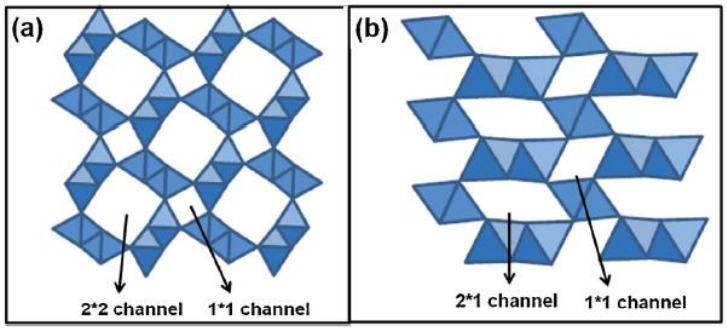

Fig. 24. Structures of (a) α-MnO_2 and (b) γ-MnO_2. (Reprinted with permission from Ref. [262]. Copyright (2016) Elsevier)

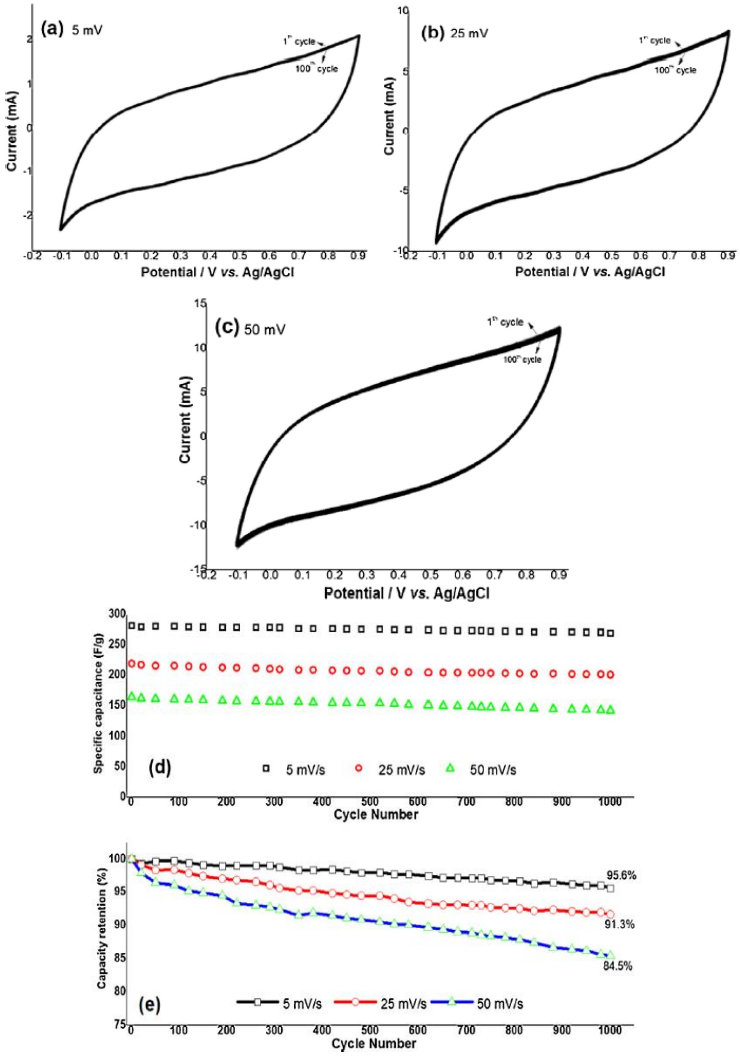

Fig. 25. (a–c) Cyclic voltammograms of the MnO_2 electrode during 1000 cycles at scan rates of 5, 10 and 50 mV s^{-1}; (d) plots of specific capacitance; and (e) capacity retention as a function of the number of charge–discharge cycles. (Reprinted with permission from Ref. [262]. Copyright (2016) Elsevier)

Our group performed CED of α-/γ-MnO_2 (Fig. 24) from a Mn nitrate bath, and this mixed MnO_2 phase exhibited a specific capacitance of 235.5 F g^{-1} and 91.3% capacity retention after 1000 cycling at 25 mV s^{-1} (Fig. 25). The applied deposition parameters were t_{on}=1s, t_{off}=1s, and I_a=2 mA cm^{-2} [263].

Pulsed cathodic deposition of MnO_2 from a nitrate bath was also performed, and the deposited MnO_2 nanorods showed a *Cs* value of 242 F g^{-1} at 2 A g^{-1} and 94.8% long-term cycling stability after 1000 cycles at 2 A g^{-1} [263]. Furthermore, α-MnO_2 nanospheres with secondary wall-like structures were fabricated by CED. The product was capable to offer a *Cs* value of 280 F g^{-1} and a 95.4% *Cs* retention after 1000 cycles [264].

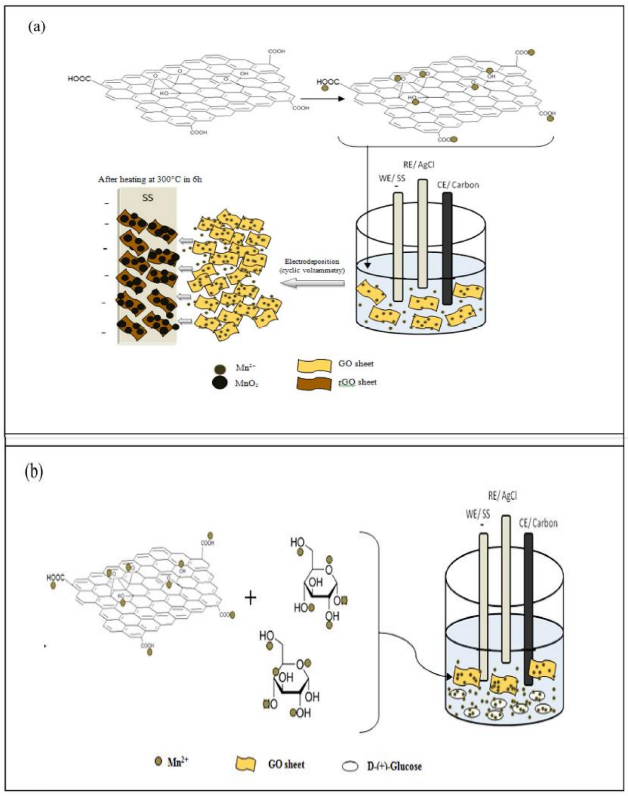

Fig. 26. A schematic illustration of rGO/MnO_2 mechanism via electrodeposition: (a) without glucose and (b) with glucose. (Reprinted with permission from Ref. [270], Copyright (2015) Nature Publishing Group)

Ag-doped MnO_2 films were coated onto steel substrate *via* galvanostatic CED method from a mixed solution of $KMnO_4$ and $AgNO_3$ in water, and a *Cs* value of 770 F g^{-1} was obtained at 2 mV s^{-1} in 0.5 M Na_2SO_4 electrolyte [265]. MnO_2 NPs were prepared *via* DC cathodic electrodeposition of MnO_2 from 0.005 M $MnCl_2$ in the presence of CTAB surfactant, and a *Cs* value of as high as 232 F g^{-1} at 0.5 A g^{-1} and 91.89% *Cs* retention were recorded for the nanoparticles [266]. Nanostructure hydrohausmannite (i.e. mixed Mn_3O_4 and MnOOH phases) was fabricated by our group using galvanostatic cathodic deposition from additive-free $MnCl_2$

bath, and capacitive parameters of *Cs*=232 F g^{-1} (at the scan rate of 5 mV s^{-1}) and 92% capacity stability after 1000 cycles were observed [267].

In the presence of CTAB, pulsed base generation (t_{on}= 1*ms*, t_{off}= 1*ms* and I_a=10 mA cm^{-2}) on the cathode surface in a two-electrode system containing 0.005 M $MnCl_2$ electrolyte was used to form a pure crystalline Mn_3O_4 with rod/particle morphology, and the fabricated electrode showed a *Cs* value 239 F g^{-1} at 2 A g^{-1}, and *Cs*=207 F g^{-1} after 1000 cycles [268].

Through a one-pot *dc* CED route, porous nanostructured Mn_3O_4 was deposited from 0.005 M $Mn(NO_3)_2$ bath [269]. The product had a high *Cs* value of 328 F g^{-1}, and preserved 95.9% of its initial *Cs* value after 1000 cycles discharging, which originated from the porous plate texture and high surface area.

CED has been also applied for decorating MnO_2 onto graphene-based nanomaterials. For example, Rusi and S. R. Majid reported the *in-situ* CED electrodeposition of binder-free rGO/MnO_2 nanocomposite electrode [270]. The electrode had an energy density of 1851 Wh kg^{-1} and a power density of 68 kW kg^{-1} at 20 A g^{-1} in a mixed KOH/$K_3Fe(CN)_6$ electrolyte. The proposed mechanism by authors for deposition of composite is presented in Fig. 26.

Beyazay *et al.* studied the cathodic electrodeposition of MnO_2 onto rGO paper [271] to form a flexible and binder-free electrode for ECs, and reported that Hausmannite-rGO is capable to storing *Cs* of 546 F g^{-1} at 0.5 A g^{-1}, and 154% capacitance retention after 10000 cycles. Moreover, porous MnO_2-MWCNT composite was deposited onto a Pt sheet using a unipolar pulse electro-deposition method. The obtained MnO_2/MWCNT composite electrode displayed a *Cs* value of 553 F g^{-1} in a 0.5 M Na_2SO_4 solution. This behavior was ascribed to the synergetic contribution of MWNTs and active MnO_2 material [272]. Chie *et al.* electrodeposited MnO_2 into a graphene hydrogel through anodic deposition, from a 2 M $Mn(CH_3COO)_2$ aqueous solution, and observed the *Cs* value of 352.9 F g^{-1} at 1 A g^{-1} and 91.5% of capacitance retention after 5000 cycles [273]. The hausmannite phase of manganese oxides was electrodeposited onto Ni mesh substrate, and the resulting electrode had a *Cs* value of 518.8 F g^{-1} at 0.1 mA cm^{-2} [274]. Jin *et al.* conducted the electrochemical deposition of MnO_2 on a flexible CNT paper and further adsorption of reduced graphene sheet (GR) on its surface to fabricate ternary MnO_2-CNT-GR composite paper. The presence of GR presence was remarkably effective in enhancing the initial *Cs* value of the composite paper from 280 F g^{-1} to 486.6 F g^{-1} [275].

Very recently, manganese oxide (MnO_2) has been incorporated with vertically aligned carbon nanotubes (VACNTs) through CED, and an improved capacitive performance was observed (i.e. *Cs* =243.3 F g^{-1} at 100 mV s^{-1}) [276]. CED has been also applied to construction of an rGO/Mn_3O_4 NPs composite [277]. In this research, GO was prepared through Hummers method, and dispersed in a Mn nitrate aqueous solution. Then, Mn_3O_4 nanoparticles were decorated onto GO sheets *via* base electrogeneration. The rGO-Mn_3O_4 nanocomposite provided *Cs* value of 364 F g^{-1} at 2 A g^{-1} and an 86.3% capacity stability after 5000

charge/discharging. Formation of the rGO/Mn_3O_4 was attributed to the electrophoretic/electrochemical deposition (EPD/ECD) mechanism (Fig. 27).

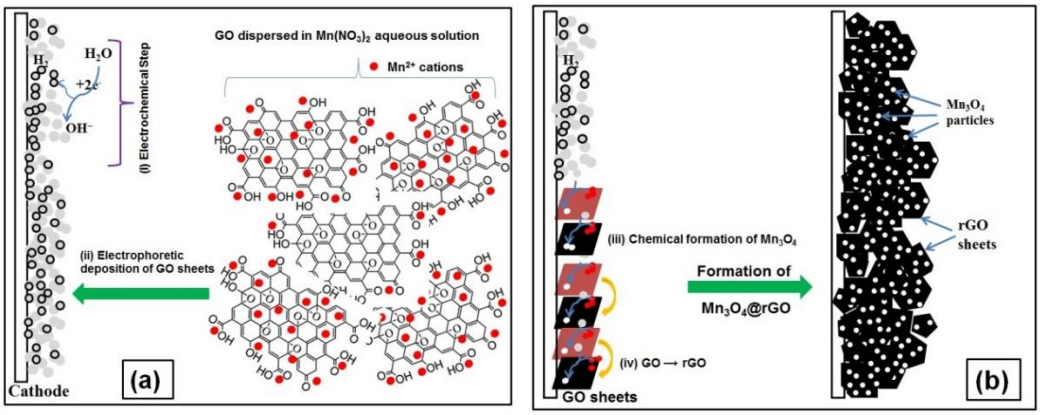

Fig. 27. Formation mechanism of rGO-Mn_3O_4 composite. (Reprinted with permission from Ref. [277]. Copyright (2018) CEE (Center of Excellence in Electrochemistry)

Gao *et al.* [278] fabricated an asymmetric supercapacitor (ASC) based on a graphene hydrogel (GH) as a negative electrode and electrodeposited MnO_2 nanoplates onto Ni foam (MnO_2-NF) as the positive electrode in aqueous Na_2SO_4 electrolyte (Fig. 28). They observed that the ASC showed reversible cycling over a wide voltage range of 0−2V, an energy density of 23.2 Wh kg^{-1},a power density of 1.0 kW kg^{-1}, and an 83.4% capacitance retention after 5000 cycles, which were enhanced in comparison with those of symmetric supercapacitors based on GH (5.5 Wh kg^{-1}) and MnO_2-NF (6.7 Wh kg^{-1}) was reported [278].

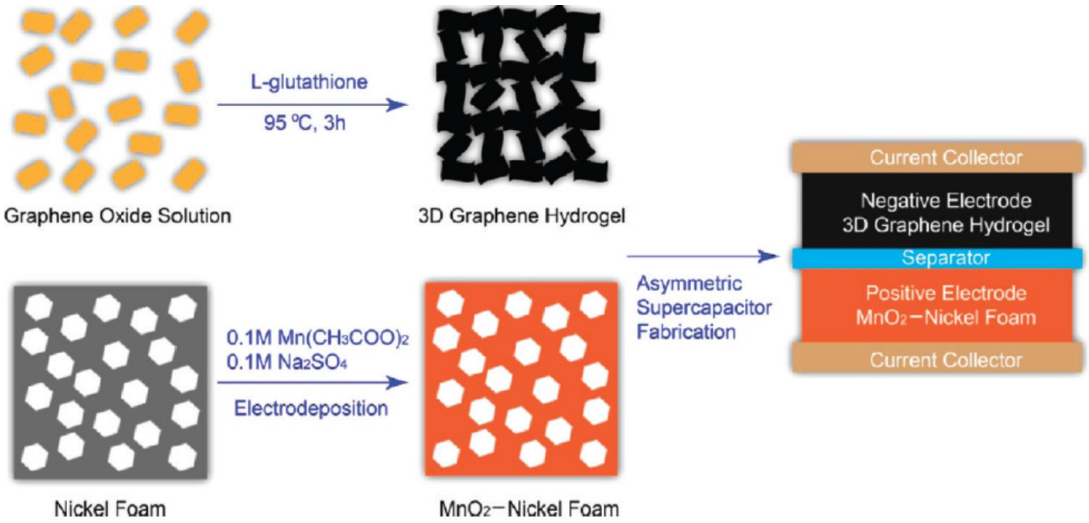

Fig. 28. Schematic illustration of the fabrication process of an asymmetric supercapacitor based on GH as the negative electrode and MnO_2-NF as the positive electrode. (Reprinted with permission from Ref. [278], Copyright (2012) American Chemical Society)

Cheng *et al.* [279] reported the decoration of MnO_2 nano-flowers onto graphene by CE deposition, and *Cs* value of 328 F g^{-1} at 1 mA and an energy density of 11.4 Wh kg^{-1} and power density of 25.8 kW kg^{-1}. Composite paper containing free-standing MnO_2 NWs deposited onto CNT paper was made by CED, and *Cs* value of 167.5 F g^{-1} at 77 mA g^{-1} and 88% retention after 3000 cycles were recorded [280]. It was mentioned that the CNT paper acted as a good conductive and active substrate for flexible SCs electrodes. The composite electrode containing carbon fabric (CF)-carbon nanotube array (CNTA)/3D porous MnO_2 nanosheets was prepared through deposition through base generation at a cathode. It was also observed that CF-CNTA/MnO_2 provides a *Cs* value 740 F g^{-1} at 2 mV s^{-1}, which is higher than that of MnO_2 electrodeposited on the stainless steel and the CF [281].

A 3D porous network MnO_2@Ni foam was prepared through potentiodynamic base generation, and led to proper *Cs* values of 2790 m F cm^{-2} (at 2 mA cm^{-2}), and 864 mF cm^{-2} (at 20 mA cm^{-2}), and 90% cycling retention after 1000 cycles at 5 mA cm^{-2} [282].

Bai *et al.* prepared flexible CNTs-MnO_2/rGO-PVDF hybrid films through layer by layer electrodeposition of MnO_2 and CNT onto rGO-PVDF/Pt sheet, and evaluated the capacitive performance of the electrode. They observed that the CNTs-MnO_2/rGO-PVDF@Pt electrode could provide a working voltage of 1.8 V accompanied by a energy density of 49.1 W h kg^{-1} at a power density of 4.83 kW kg^{-1} [283]. MnO_2/rGO composites were grown on carbon cloth through a one-step electrochemical deposition, showing an area capacitance of 14 F cm^{-2} at 2 mV s^{-1} and excellent stability [284].

Zhu *et al.* used CED as a one-step electrochemical method to prepare graphene/MnO_2 nanowall hybrids (GMHs). They performed CED experiments in a 0.1 M Na_2SO_4/0.05 M $Mn(OAc)_2$ bath and found that graphene oxide (GO) could beelectrochemically reduced into graphene in the deposition of MnO_2 nano-walls through base generation at the cathode surface [285]. MnO_2/G/NF composite was fabricated by the electrophoretic deposition (EPD) of graphene onto NF (EPD-G/NF) and the electrodeposition of MnO_2 on EPD-G/NF (MnO_2/EPD-G/NF). The MnO_2/EPD-G/NF composite exhibited a *Cs* value of 476 F g^{-1} at 1 A g^{-1} in 0.5M Na_2SO_4 [286].

Yu *et al.* [287] developed CED as a scalable solution-based route to fabricate graphene/MnO_2 electrode, and observed that an efficient use of MnO_2 nanomaterials in capacitive tests is possible in the presence of graphene.

Using a one-step co-electrodeposition method (i.e. EDP-ECD), MnO_2/PEDOT coaxial nanowires were constructed as an SC electrode, where a good capacitance ability with 85% *Cs* retention was observed for these coaxial nanowires [288]. Zhang *et al.* [289] fabricated a 3D hierarchical rGO/MnO_2/carbon foam nanocomposite using CED method, and observed a high *Cs* value of 356.5 F g^{-1} at 10 mV s^{-1}, and retained 93.6% of the original *Cs* after 2000. Also, a freestanding 3D graphene/MnO_2 composite was fabricated through CED by He *et al.* [290]. Kazemi *et al.* [291] electrodeposited MnO_2 nanostructures onto Ni foam decorated with copper

NPs, and observed area capacitance of 557 mF cm^{-2} and *Cs* of 687 F g^{-1} for the prepared electrode. Also, they found that the morphology and size of the deposited MnO_2 depended on the Cu deposition time. Tsai *et al.* performed potentiodynamic (PD), potentiostatic (PS), and a combination of PS and PD (PS+PD) electrodeposition modes in a 0.1 M $Mn(CH_3COO)_2$ and 0.1 M Na_2SO_4 electrolyte, and prepared three kinds of hierarchical meso/macroporous MnO_2/Ni foam electrodes [292]. They found that (i) the deposition mode markedly effects the surface morphology, texture, and SC properties of the MnO_2/Ni electrode, and (ii) that the so-prepared MnO_2/Ni fabricated exhibits superior charge storage ability as compared with those prepared *via* PD and PS modes. This electrode (i.e. AC)//(MnO_2/Ni)) exhibited an energy density of 7.7 Wh kg^{-1} at a power density of 600 W kg^{-1} and 98% cycling stability after 10000 cycles in an asymmetric supercapacitor set-up with activated carbon. This suitable SC performance was attributed to the high surface area, hierarchical structure, and interconnected 3D reticular configuration of the deposited MnO_2.

2.3. Mixed metal oxides and hydroxides

Transition metal oxides/hydroxides (TMOHs) exhibit promising pseudocapacitance charcateristics both in aqueous and non-aqueous electrolytes due to their high theoretical capacities [293]. Binary metal oxides (BMOs) contain at least one transition M^{n+} and one or more electrochemically active/inactive ions. BMOs can display synergistic effects, which result in an enhanced charge storage performance with greater practical potential window, superior conductivity, high electrochemical usage and improved cycle life [294-298]. Binary metal oxides possessing multiple oxidation states have exhibited higher supercapacitive performance than single component metal oxides. This enables multiple redox reactions during electrochemical reactions. For example, $NiCo_2O_4$, $ZnCo_2O_4$, $CuFe_2O_4$, $CuMn_2O_4$, and etc. with achievable oxidation states that enable multiple redox reactions and high electrical conductivities have been widely studied [299-311]. Ternary metal oxides (TMOs) with the general formula of $A_xB_yO_z$ include several types of AB_2O_4, ABO_4, and $A_3B_2O_8$, etc., where A and B represent the metal elements having low and high oxidation states, respectively. When TMOs are used in capacitor electrodes, both A and B metals contribute to the faradic redox reaction and the delivered pseudo-capacitive energy storage values [302-304]. Up to now, various chemical methods like as hydrothermal, solvothermal, precipitation, thermal decomposition, etc. have been developed to fabricate both binary and ternary metal oxides [305-312], and various nanostructures of these oxides including particles, plates, rods, spheres, tubes, and so on, have been prepared and investigated as electrode materials for supercapacitors uses [313-322]. Electrodeposition is an easy method for fabricating BMOs and TMOs, which provides amazing advantages compared with other preparation routes including one-step and tailor-mode synthetic procedures, short times, and inexpensive and safe reagents [323-325]. As an electrodeposition route, cathodic deposition *via* base generation has been used by many

researchers for fabricating mixed metal oxides (i.e. BMOs and TMOs) at nanoscale and the obtained electrodes were studied as charge storage system. For example, Mirzaee *et al.* [326] deposited Ni,Co hydroxides onto an ERGO/Ni-NiO substrate *via* the potentiostatic base generation strategy and after heat-treatment at 300°C, flower-like $NiCo_2O_4$ was obtained. They found that flower-like 3D $NiCo_2O_4$ could be manipulated by changing the deposition potential, where at the optimized potential (i.e. −1.0 V *vs*. SCE), the fabricated composite exhibited the highest surface area (SA=85 m^2 g^{-1}), Cs of 2461 F g^{-1} and 94% stability after 4000 cycles [326]. The following mechanism has explained for $NiCo_2O_4$ formation [312,325,326]:

(i) Base generation step on the Ni foam:

$$NO_3^- + 7H_2O + 8e^- \rightarrow NH_4^+ + 10OH^- \quad (18)$$

(ii) Forming the MHs precursor:

$$Ni^{2+} + 2Co^{2+} + 6OH^- + NiCo_2(OH)_6 \quad (19)$$

(ii) Heat treatment:

$$NiCo_2(OH)_6 + 12O_2 \rightarrow NiCo_2O_4 + 3H_2O \quad (20)$$

Ghassemi *et al.* [327] performed constant current cathodic electrosynthesis of a $CuFe_2O_4$/CuO composite *via* base generation route, and observed the *Cs* value of 322.49 F g^{-1} at the scan rate of 1 mV s^{-1}, and 92% capacitance retention after 5000 cycles. $ZnMn_2O_4$ nanosheets have been also synthesized through a base generation strategy (i.e. CED method), followed by HT process, as presented in Fig. 29 [328], where a galvanostatic CED of Zn–Mn hydroxide was coated on both sides of the aqueous 0.005M $Zn(NO_3)_2$ /0.01M $Mn(NO_3)_2$ bath. The prepared nanosheets exhibited a *Cs* of 457 F g^{-1} at 1 A g^{-1}, 67.2% capacity retention at 10 A g^{-1}, and 92.5% *Cs* loss after 4000 cycles at 3 A g^{-1}.

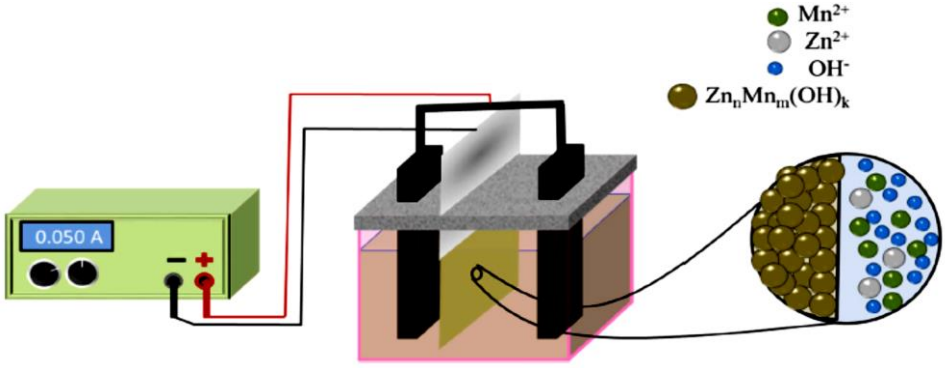

Fig. 29. Schematic representation of the preparation of $ZnMn_2O_4$. (Reprinted with permission from Ref. [328], Copyright 2019 Springer)

$CuCo_2O_4$ nanosheets @Ni foam were fabricated through the potentiostatic base generation method followed by calcination at 300 ºC for 2h, and the effects of the deposition time and salt type (Co,Cu nitrate or Co,Cu chloride) on the $CuCo_2O_4$ morphology were studied [329]. The optimum conditions were found to be $t_{deposition}$=10 min, and salt type=nitrate, where the fabricated $CuCo_2O_4$ electrode at these conditions showed complete uniform and ultra-thin nano-sheet arrays, high capacitance (*Cs*=1330 F g^{-1} at 2 A g^{-1}), 70% *Cs* retention at ultrahigh load of 60 A g^{-1}, and 93.6% stability after 5000 cycles.

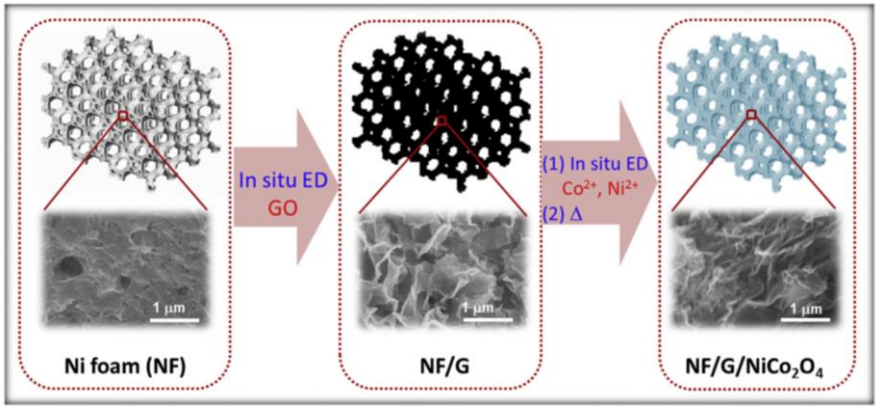

Fig. 30. Illustrative fabrication process toward the NF/G/$NiCo_2O_4$ electrode. (Reprinted with permission from Ref. [331], Copyright (2015) Elsevier)

Mn_3O_4-NiO-Co_3O_4 nanostructure/SS composite electrode was prepared using CED followed by calcination at 300 ºC for 6h. The ternary oxide composite showed a *Cs* of 7404 F g^{-1} with a high energy and power density of 1028 Wh kg^{-1} and 99 kW kg^{-1} at 20 A g^{-1} [330]. Nguyen *et al* fabricated $NiCo_2O_4$/G/NF through the following steps (as shown in Fig. 30) [331]: (i) electrophoretic (ED) decoration of graphene sheets onto Ni foam, which formed G/NF electrode, (ii) CED preparation of bimetallic (Ni, Co) hydroxide precursor onto G/NF electrode *via* potentiostatic base generation, and (iii) calcination at 300 ºC for 2 h. They observed that the electrode delivers a *Cs* of 1950 F g^{-1} at a high current density of 7.5 A g^{-1}.

3D $NiCo_2O_4$/N-CNTs Ni foam electrode was constructed through successive three steps of (i) CVD, (ii) cathodic deposition *via* base generation, and (iii) calcination at 300 ºC for 2h [332]. The resulting electrode showed a high Cs of 1472 F g^{-1} (at 1 A g^{-1}), s remarkable rate capability and 99% capacity retention after 3000 cycles. Mesoporous $Mn_{1.5}Co_{1.5}O_4$ spinel films were also directly deposited onto an Ni foam by cathodic deposition *via* base generation, and calcination at 400 ºC for 2 h, and exhibited an energy density of 27.6 Wh kg^{-1} and a power density of 1.01 kW kg^{-1} at 1 Ag^{-1} [333]. Rusi *et al* deposited MnO_2-NiO binary oxide electrode from 0.25 M $Ni(CH_3COO)_2.4H_2O$+0.01 M $Mn(CH_3COO)_2.4H_2O$ using base generation at stainless steel surface and then calcination at 300 ºC for 6h [334]. They observed *Cs* values of 435 F g^{-1} and 681 F g^{-1} with an energy density of 242 Wh kg^{-1} and 213 Wh kg^{-1} in 0.5 M

Na_2SO_4 and 0.5M KOH electrolyte, respectively. Heydari *et al.* directly deposited $ZnCo_2O_4$ nanoflakes on Ni foam *via* base generation followed by calcination at 400 ºC for 2h. The prepared electrode had a mesoporous texture with a large SA of 138.8 $m^2\ g^{-1}$, with a proper *Cs* of 1781.7 F g^{-1} at 5 A g^{-1}, and 62% capacity retention at 50 A g^{-1} [335]. $ZnMn_2O_4/Mn_3O_4$ composite were also prepared by galvanostatic base generation on a steel cathode surface followed by heat-treatment at 300 ºC for 2 h, which showed specific capacitance of 321.34 F g^{-1} at 1 mV s^{-1}, and 93% cycling stability after 2000 cycles [336].

Yan *et al.* performed cathodic electrodeposition of bimetallic (Ni,Co) hydroxide onto Ni foam from a 0.004 M $Co(NO_3)_2$/0.002 M $Ni(NO_3)_2$ aqueous electrolyte and then heat-treated the hydroxide deposit at 300 °C for 2 h, to obtain ultrathin mesoporous $NiCo_2O_4$ nanosheets. An ultra-high *Cs* of 1450 F g^{-1} at high load of 20 A g^{-1} was observed for the fabricated electrode [337], which was related this good performance to the ultrathin mesoporous texture of nanosheets, where fast electron and ion transport and large SA are possible, and there is excellent structural stability during cycling. Around the same way, porous $NiCo_2O_4$ nanosheets were deposited onto flexible carbon fabric (CF) by Du *et al.*, and specific capacitance of 2658 F g^{-1} at 2 A g^{-1} has seen for this electrode [338]. Co,Al-LDH and Co,Fe-LDH have been electro-synthesized on Pt electrodes via base generation strategy, and Cs values of 854 and 869 F g^{-1} at 1 A g^{-1} were exhibited by these electrodes, respectively [339].

Shao *et al.* [340] applied potentiostatic CED followed by calcination at 350 ºC for 2 h to prepare $NiCo_2O_4$–GO coated onto Ni foam. The *Cs* was 1078 F g^{-1} at 1 mA and a great cyclic stability was observed and its excellent charge storage action were attributed to the hierarchical porous nano-sheet-like unique structure of electro-synthesized materials. Beside binary and ternary metal oxides (BMOs and TMOs), layered double hydroxides (LDHs) are fascinating candidates for use in charge storage devices. LDHs are a 2D anionic clays composed of positively charged brucite-like host layers and exchangeable charge-balancing interlayer anions, which can be formulated as $[M^{2+}_{1-x}M^{3+}_{x}(OH)_2]^{x+}(A^{n-})_{x/n}.mH_2O$ [341,342]. In this structure, some M^{2+} cations are octahedrally linked to OH^- groups, and some M^{2+} cations has uniformly substituted by M^{3+} with *x* value of between 0.2 and 0.4 [343]. These LHD structures were considered as promising SC electrodes due to their relatively fast faradic reactions, environmental friendly nature and effective electrochemical contribution of metal cations. Potentiostatic/galvanostatic cathodic electrodeposition (P/G-CED) *via* base generation has been also applied to prepare layered double hydroxides (LDHs). For example, 3D Ni–Co LDHs was directly deposited on Ni foam by successive CED method, and the fabricated electrode showed a high *Cs* of 1760 F g^{-1} and over 62.5% rate capability at current load rage of 1–100 A g^{-1} [344]. A Co_xNi_{1-x}-LDHs/N-doped CNTs/Ni foam electrode was simply fabricated by Wu *et al.* using a combination of CVD/CED methods, and they observed that this electrode displays a remarkable storage ability capacitance (*Cs*=2170 F g^{-1} at 1 A g^{-1} and C_{areal}=1.62 F cm^{-2} at 1 mA cm^{-2}), 80.9% *Cs* retention at 20 A g^{-1} and 75.8% C_{areal} retention at 30 mA cm^{-2} [345]. An

$Co_{0.66}Ni_{0.34}$-LDHs electrode was also prepared by potentiodynamic CED route, and a proper capacitive capability was delivered by this system i.e. Cs=1213 F g^{-1}, E=104 Wh kg^{-1}, P=1.44 kW kg^{-1} and cycle life=77% after 10000 cycles [346].

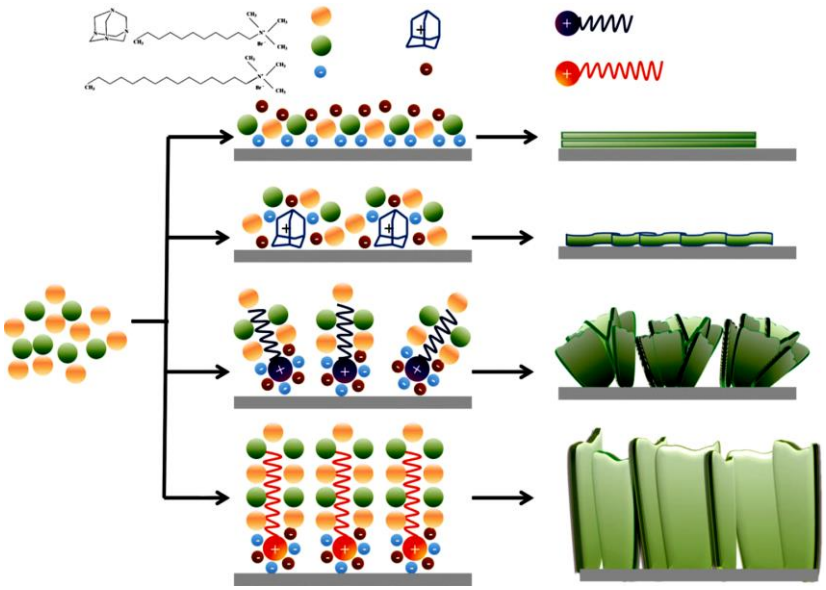

Fig. 31. (a) Molecular structures of selected surfactants; (b) the possible formation mechanism of $Co_{0.75}Ni_{0.25}(OH)_2$ LDHs supported on the nickel foam substrate. (Reprinted from Ref. [347] with permission from RSC Publications)

In the same way, cauliflower-like $Co_{0.75}Ni_{0.25}(OH)_2$ was successfully obtained via cathodic electrodeposition in the DTAB or CTAB surfactants presence [347]. It was observed that tailoring the morphology of the deposited CoNi-LDH is achievable in the presence of a surfactant as an additive. In fact, the deposited CoNi-LDHs with DTBA and CTAB surfactants showed wrinkle-like, cauliflower-like or net-like structures (Fig. 31).

A layered $Ni_{0.5}Co_{0.5}(OH)_2$ film onto stainless steel was easily prepared by base generation strategy, and a specific capacity of 762 C g^{-1} at 1 A g^{-1} was reported of this electrode [348]. Li *et al.* reported the electrochemical synthesis of MXene/NiCo-LDH mixture onto Ni foam. They first deposition of Ti_3C_2 onto Ni foam by immersion procedure, and then the deposited bimetallic hydroxide (i.e. Ni,Co-LDH) onto Ti_3C_2@Ni foam in a 0.01 M cobalt nitrate+0.005 M nickel nitrate aqueous bath. The prepared NiCo-LDH/Ti_3C_2@Ni foam electrode exhibited *Cs* of 983.6 F g^{-1} at 2 A g^{-1} and 76% retention after 5000 cycles at 30 A g^{-1} [349].

Binary $Ni_xCo_{1-x}(OH)_2$ hydroxides were coated onto graphite substrate by Chen *et al.* [350] through base generation on the cathode surface (i.e. CED method), and the deposition parameters were systematically investigated and reported. They found that (i) the applied deposition current dedicate the morphology of hydroxides, (ii) porous microstructures are formed at low current, and (iii) bath temperature and pH determine the Co/Ni ratio of

hydroxide. The fabricated $Ni_{0.32}Co_{0.68}(OH)_2$/graphite electrode showed a *Cs* of 1000 F g^{-1} at 5 mV s^{-1}, and 100% capacitance retention after 1000 cycles [351]. Using cathodic deposition through base generation, $Ni_{0.5}Co_{0.5}(OH)_2$ nanosheets were also grown onto $CuCo_2O_4$ nano-needle arrays, which gave rise to a composite core/shell electrode with a superior capacity of 295.6 mAh g^{-1} at 1 A g^{-1} and 220 mAh g^{-1} at 40 A g^{-1} [351]. Similarly , CoNi-LDHs@ nickel foam electrode was made by Wei *et al.* [352], and at the optimized Co/Ni molar ratio of 0.64/0.36, they observed the capacitance of 1587.5 F g^{-1} at 0.5 A g^{-1} and 91.5% cycling stability after 1000 cycles at 5 A g^{-1}. The composite Ni-Co LDH/rGO/NF was prepared through potentiodynamic base generation in a $Co(NO_3)_2$ $6H_2O$/$Ni(NO_3)_2$ $6H_2O$/CTAB electrolyte. GO was prepared by a simple immersion method. It has been reported that the presence of CTAB leads to the formation of ultra-thin nanosheets. The specific capacitance of 2133.3 F g^{-1} at 4 A g^{-1} was delivered by Ni-Co LDH/rGO/NF electrode [353].

3. CONCLUSION AND OUTLOOK

Cathodic electrochemical deposition (CED) provides simple, facile and high efficient procedure for the synthesis of nanostructured metal oxides/hydroxides (MOHs) and their composites with graphene-based material. Different 1D, 2D and 3D nanostructures of MOHs including nanotubes, nanoplates, nanorods, nanowires, nanoflakes, nanocapsules, structures, and multi-component composite nano-electrodes with high surface can be easily fabricated through one-step or successive cathodic deposition. The performance of electrochemical energy nanomaterials strongly depends on their nanostructures and compositions. Results of research reports indicate that cathodic electrodeposition *via* base generation on the cathode surface provides the one-step, easy and short route for the fabrication of metal oxides/hydroxides and their composites onto any conductive substrate, which can be directly used as electrode for supercapacitors. Furthermore, this technique presents the following additional advantages: (a) the only simple bath containing metal nitrate/chloride is needed, (b) simple/mild synthesis conditions, (c) avoiding high temperature/pressure, (d) manipulate the size, morphology, phase and composition of products through manual variables like current and voltage, (e) applicable with different modes of CC, PD, Each of PC and CV offers its own advantage and (f) give high pure products.

To achieve high performance MOHs composite electrodes, high surface area, porous and multi-layered nanostructures should be designed and fabricated. Accordingly, many efforts have been made to apply cathodic electrodeposition for preparing high performance composites based on the metal oxides/hydroxides nanomaterials, and considerable progress has been reported. Nevertheless, some issues need to be considered more in the application of CED to form MOHs and their composites. First, pulse and pulse reverse cathodic electrodeposition *via* base generation has been rarely applied in the synthesis of these oxides and hydroxides, although the morphology and size of the deposited electro-active materials could be easily

tailored *via* these modes. Second, hydrogen bubbling has been rarely studied in the cathodic electrodeposition *via* base generation of metal oxides/hydroxides, where dynamic hydrogen bubble template (DHBT) could be used for design and fabrication of completely porous and high surface area oxides/hydroxides. Third, since MOHs show poor electric conductivity, their composites with various carbon materials could provide better conductivity and capacitive performances. These materials include graphene, rGO, mesoporous carbon (CMK), graphitic carbon nitride (g-C_3N_4), porous graphene, N,S-doped graphene, functionalized CNTs, and mixed of these materials. However, among these carbonous materials, one-step electrodeposition of graphene (rGO, ERGO)/metal oxides(hydroxides) composites have been subject of many reports. Hence, CED of other carbon-based material with oxides/hydroxides should be considered and investigated more.

REFERENCES

[1] Q. Li, S. Zheng, Y. Xu, H. Xue, and H. Pang, Chem. Eng. J. 333 (2018) 505.
[2] H. Over, Electrochim. Acta 93 (2013) 314.
[3] M. Rahimi-Nasrabadi, S. M. Pourmortazavi, M. Sadeghpour Karimi, M. Aghazadeh, M. R. Ganjali, and P. Norouzi, J. Mater. Sci.: Mater. Electron. 28 (2017) 6399.
[4] M. Rahimi-Nasrabadi, S. M. Pourmortazavi, M. S. Karimi, M. Aghazadeh, M. R. Ganjali, and P. Norouzi, J. Mater. Sci.: Mater. Electron. 28 (2017) 15224.
[5] H. M. Shiri, A. Ehsani, and M. J. Khales, J. Coll. Interface Sci. 505 (2017) 940.
[6] M. Rahimi-Nasrabadi, S. M. Pourmortazavi, M. Aghazadeh, M. R. Ganjali, M. Sadeghpour Karimi, and P. Norouzi, J. Mater. Sci. Mater. Electron. 28 (2017) 5574.
[7] L. Chen, X. Guo, W. Lu, M. Chen, Q. Li, H. Xue, and H. Pang, Coor. Chem. Rev. 1 (2018) 13.
[8] M. Rahimi-Nasrabadi, S. M. Pourmortazavi, M. Aghazadeh, M. R. Ganjali, M. Sadeghpour Karimi, and P. Norouzi, J. Mater. Sci.: Mater. Electron. 28 (15) 11383.
[9] H. M. Shiri, and A. Ehsani, Bull. Chem. Soc. Jpn. 89 (2016) 1201.
[10] R. S. Kate, S. A. Khalate, and R. J. Deokate, J. All. Compd. 734 (2018) 89.
[11] L. Ji, C. Lv, Z. Chen, Z. Huang, and C. Zhang, Adv. Mater. 30 (2018)1705653.
[12] M. Rahimi-Nasrabadi, S. Mahdi. Pourmortazavi, M. Aghazadeh, M. R. Ganjali, M. Sadeghpour Karimi, and P. Novrouzi, J. Mater. Sci.: Mater. Electron. 28 (2017) 9478.
[13] J. Torabian, M. G. Mahjani, H. M. Shiri, A. Ehsani, and J. S. Shayeh, RSC Adv. 6 (2016) 41045.
[14] S. Mahdi. Pourmortazavi, M. Rahimi-Nasrabadi, M. Aghazadeh, M. R. Ganjali, M. Sadeghpour Karimi, and P. Novrouzi, J. Mol. Struc. 1150 (2017) 411.
[15] H. M. Shiri, and A. Ehsani, J. Collid Interface Sci. 495 (2017) 102.
[16] M. Rahimi-Nasrabadi, S. Mahdi. Pourmortazavi, M. Aghazadeh, M. Sadeghpour Karimi, M. R. Ganjali, and P. Norouzi, J. Elec. Mater. 46 (2017) 4627.

[17] H. M. Shiri, and A. Ehsani, J. Collid Interface Sci. 473 (2016) 126.
[18] M. Rahimi-Nasrabadi, S. M. Pourmortazavi, M. Sadeghpour Karimi, M. Aghazadeh, M. R. Ganjali, and P. Norouzi, J. Mater. Sci.: Mater. Electron. 28 (2017) 13267.
[19] J. M. Xu, and J. P. Cheng, J. Alloy Compd. 686 (2016) 753.
[20] M. Rahimi-Nasrabadi, S. Mahdi. Pourmortazavi, M. Aghazadeh, M. R. Ganjali, M. Sadeghpour Karimi, and P. Norouzi, J. Mater. Sci.: Mater. Electron. 28 (2017) 3780.
[21] H. M. Shiri, and A. Ehsani, J. Colloid Interface Sci. 484 (2016) 70.
[22] K. M. Lee, C. W. Lai, K. S. Ngai, and J. C. Juan, Water Res. 88 (2016) 428.
[23] C. B. Ong, L. Y. Ng, and A. W. Mohammad, Renewable Sustainable Energy Rev. 81 (2018) 536.
[24] T. Montini, M. Melchionna, M. Monai, and P. Fornasiero, Chem. Rev. 116 (2016) 5987.
[25] M. Gong, D. Y. Wang, Ch. Ch. Chen, B. J. Hwang, and H. Dai, Nano Res. 9 (2016) 28.
[26] J. Wang, W. Cui, Q. Liu, Z. Xing, A. M. Asiri, and X. Sun, Adv. Mater. 28 (2016) 215.
[27] L. Mohapatra, and K. Parida, J. Mater. Chem. A 4 (2016) 10744.
[28] H. Yin, and Z. Tang, Chem. Soc. Rev. 45 (2016) 4873.
[29] A. Sobhani-Nasab, M. Behpour, M. Rahimi-Nasrabadi, F. Ahmadi, Ultrason. Sonochem. 50 (2019) 46.
[30] J. P. Cheng, J. Zhang, and F. Liu, RSC Adv. 4 (2014) 38893.
[31] A. Sobhani-Nasab, S. Pourmasoud, F. Ahmadi, M. Wysokowski, T. Jesionowski, H. Ehrlich, and M. Rahimi-Nasrabadi, Mater. Lett. 238 (2019) 159.
[32] M. Zhao, Q. Zhao, B. Li, H. Xue, H. Pang, and C. Chen, Nanoscale 9 (2017) 15206.
[33] M. Rahimi-Nasrabadi, H. Ehrlich, and F. Sedighi, J. Mater. Sci.: Mater. Electron. 29 (2018) 11081.
[34] H. Kooshki, A. Sobhani-Nasab, M. Eghbali-Arani, F. Ahmadi, and V. Ameri, Separation Purification Technol. 211 (2019) 873.
[35] A. González, E. Goikole, J. A. Barrena, and R. Mysyk, Renewable Sustainable Energy Rev. 58 (2016) 1189.
[36] F. Wang, X. Wu, X. Yuan, Z. Liu, Y. Zhang, and L. Fu, Chem. Soc. Rev. 46 (2017) 6816.
[37] S. M. Pourmortazavi, M. Rahimi-Nasrabadi, M. Aghazadeh, M. R. Ganjali, M. Sadeghpour Karimi, and P. Norouzi, Mater. Res. Express 4 (2017) 035012.
[38] M. Zhi, C. Xiang, J. Li, M. Li, and N. Wu, Nanoscale 5 (2013) 72.
[39] D. Chen, Q. Wang, R. Wang, and G. Shen, J. Mater. Chem. A 3 (2015) 10158.
[40] S. M. Pourmortazavi, M. Rahimi-Nasrabadi, F. Ahmadi, and M. R. Ganjali, J. Mater. Science: Mater. Electron. 29 (2018) 9442.
[41] Ch. Zhong, Y. Deng, W. Hu, J. Qiao, L. Zhang, and J. Zhang, Chem. Soc. Rev. 44 (2015) 7484.

[42] X. Xia, Y. Zhang, D. Chao, C. Guan, Y. Zhang, L. Li, X. Ge, I. Mínguez Bacho, J. Tu, and H. J. Fan, Nanoscale 6 (2014) 5008.
[43] F. Wang, X. Wang, Z. Chang, Y. Zhu, L. Fu, X. Liua, and Y. Wu, Nanoscale Horiz. 1 (2016) 272.
[44] G. R. Li, H. Xu, X. F. Lu, J. X. Feng, Y. X. Tong, and C. Y. Su, Nanoscale 5 (2013) 4056.
[45] L. Tsui, and G. Zangari, Electrochemical Synthesis of Metal Oxides for Energy Applications. In: Djokić S. (eds) Electrodeposition and Surface Finishing. Modern Aspects of Electrochemistry, Springer, New York Vol. 57. (2014).
[46] M. Aghazadeh, J. Electrochem. Soc. 159 (2012) E53.
[47] M. Aghazadeh, M. Ghaemi, A. N. Golikand, and A. Ahmadi, Mater. Lett. 65 (2011) 2545.
[48] M. Aghazadeh, and M. Hosseinifard, Ceram. Int. 39 (2013) 4427.
[49] M. Aghazadeh, A. A. Malek Barmi, H. M. Shiri, and S. Sedaghat, Ceram. Int. 39 (2013) 1045.
[50] A. A. Malek Barmi, M. Aghazadeh, and H. M. Shiri, Russian J. Electrochem. 49 (2013) 583.
[51] F. Khosrow-pour, M. Aghazadeh, S. Dalvand, and B. Sabour, Mater. Lett. 104 (2013) 61.
[52] M. Aghazadeh, Mater. Lett. 211 (2018) 225.
[53] M. Aghazadeh, A. N. Golikand, M. Ghaemi, and T. Yousefi, Mater. Lett. 65 (2011) 1466.
[54] M. Aghazadeh, M. Hosseinifard1, M. H. Peyrovi, and B. Sabour, J. Rare Earths 31 (2013) 281.
[55] M. Aghazadeh, and T. Yousefi, Mater. Lett. 73 (2012) 176.
[56] M. Aghazadeh, B. Arhami, A. A. M. Barmi, M. Hosseinifard, and D. Gharailou, Mater. Lett. 115 (2014) 68.
[57] I. Karimzadeh, H. Rezagholipour Dizaji, and M. Aghazadeh, Mater. Res. Express 3 (2016) 095022.
[58] F. Abed, M. Aghazadeh, and B. Arhami, Mater. Lett. 99 (2013) 11.
[59] F. Khosrow-pour, M. Aghazadeh, B. Sabour, and S. Dalvand, Ceram. Int. 39 (2013) 9491.
[60] G. H. Annal Therese, and P. Vishnu Kamath, Chem. Mater. 12 (2000) 1195.
[61] I. Zhitomirsky, Adv. Colloid Interface Sci. 97 (2002) 279.
[62] I. Karimzadeh, M. Aghazadeh, M. R. Ganjali, P. Norouzi, S. Shirvani-Arani, T. Doroudi, P. H. kolivand, S. A. Marashi, and D. Gharailou, Mater. Lett. 179 (2016) 5.
[63] M. Aghazadeh, M. R. Ganjali, and P. Norouzi, Mater. Res. Express 3 (2016) 055013.
[64] M. Aghazadeh, I. Karimzadeh, and M. R. Ganjali, Mater. Lett. 228 (2018) 137.

[65] M. Hosseini, M. Aghazadeh, and M. R. Ganjali, New J. Chem. 41 (2017) 12678.
[66] I. Karimzadeh, H. R. Dizaji, and M. Aghazadeh, J. Magn. Magn. Mater. 416 (2016) 81.
[67] M. R. Ganjali, and M. Rezapour, Aanal. Bioanal. Electrochem. 10 (2018) 901.
[68] M. Aghazadeh, and I. Karimzadeh, Curr. Nanosci. 14 (2018) 42.
[69] M. Aghazadeh, I. Karimzadeh, M. R. Ganjali, and M. Mohebi Morad, Mater. Lett. 196 (2017) 392.
[70] M. R. Ganjali, E. Pourbasheer, and M. Rezapour, Aanal. Bioanal. Electrochem. 10 (2018), 394
[71] I. Karimzadeh, M. Aghazadeh, M. R. Ganjali, P. Norouzi, T. Doroudi, and P. H. Kolivand, Mater. Lett. 189 (2017) 290.
[72] M. Aghazadeh, M. G. Maragheh, M. R. Ganjali, and P. Norouzi, Inorg. Nano-Metal Chem. 27 (2017) 1085.
[73] M. Aghazadeh, I. Karimzadeh, and M. R. Ganjali, Curr. Nanosci. 15 (2019) 169.
[74] R. Cheraghali, and M. Aghazadeh, Anal. Bioanal. Electrochem. 8 (2016) 64.
[75] I. Karimzadeh, M. Eslami, and V. Moghaddam, Anal. Bioanal. Electrochem. 11 (2019) 70.
[76] M. Aghazadeh, A. Nozad Golikand, M. Ghaemi, and T. Yousefi, J. Electrochem. Soci. 158 (2011) E136.
[77] M. Aghazadeh, Anal. Bioanal. Electrochem. 10 (2018) 508.
[78] M. Aghazadeh, A. Nozad, H. Adelkhani, and M. Ghaemi, J. Electrochem. Soc. 157 (2010) D519.
[79] M. Aghazadeh, A. A. Malek Barmi, and H. Mohammad Shiri, Russian J. Electrochem. 49 (2013) 344.
[80] M. Aghazadeh, A. A. Malek Barmi, and M. Hosseinifard, Mater. Lett. 73 (2012) 28.
[81] I. Karimzadeh, M. Aghazadeh, T. Doroudi, M. R. Ganjali, and D. Gharailou, J. Cluster Sci. 28 (2017) 1259.
[82] T. Yousefi, M. Aghazadeh, A. N. Golikand, and M. H. Mashadizadeh, Sci. Adv. Mater. 4 (2012) 214.
[83] M. Aghazadeh, and K. Yavari, Anal. Bioanal. Electrochem. 10 (2018) 1426.
[84] F. Khosrow-pour, M. Aghazadeh, and B. Arhami, J. Electrochem. Soc. 160 (2013) D150.
[85] B. Li, M. Zheng, H. Xue, and H. Pang, Inorg. Chem. Front. 3 (2016) 175.
[86] O. Guiaderz, and P. Bernard, J. Electrochem. Soc. 165 (2018) A396.
[87] M. Aghazadeh, A. N. Golikand, and M. Ghaemi, Int. J. Hydrogen Energy 36 (2011) 8674.
[88] G. Fu, Z Hu, L. Xie, X. Jin, Y.u Xie, Y. Wang, Z. Zhang, Y. Yang, and H. Wu, Int. J. Electrochem. Sci. 4 (2009) 1052.
[89] R. Yuksel, S. Coskun, Y. E. Kalay, and H. E. Unalan, J. Power Sour. 328 (2016) 167.

[90] Y. Wu, Shangbin Sang, W. Zhong, F. Li, K. Liu, H. Liu, Z. Lu, and Q. Wu, Electrochim. Acta 261 (2018) 58.
[91] M. Aghazadeh, B. Sabour, M. R. Ganjali, and S. Dalvand, Appl. Surf. Sci. 313 (2014) 581.
[92] S. Guangjie, Y. Yue, Z. Shipin, and H. E. Pei, Rare Metals 28 (2009) 132.
[93] Y. Zheng, S. Kui, W. Zhicheng, W. Xiaofeng, and K. Xianghu, Appl. Surf. Sci. 258 (2012) 8117.
[94] M. Aghazadeh, M. Ghaemi, B. Sabour, and S. Dalvand, J. Solid State Electrochem. 18 (2014) 1569.
[95] L. Aguilera, Y. Leyet, R. Peña-Garcia, E. Padrón-Hernández, R. R. Passos, and L. A. Pocrifka, Chem. Phys. Lett. 677 (2017) 75.
[96] J. Tizfahm, B. Safibonab, M. Aghazadeh, A. Majdabadi, and B. Sabour, Colloids Surf. A 443 (2014) 544.
[97] I. H. Lo, J. Y. Wang, K. Y. Huang, J. H. Huang, and W. P. Kang, J. Power Sour. 308 (2016) 29.
[98] Z. Zeng, P. Sun, J. Zhu, and X. Zhu, Surf. Interfaces 8 (2017) 73.
[99] Z. Yang, C. Fang, Y. Fang, Y. Zhou, and F. Zhu, Int. J. Electrochem. Sci. 10 (2015) 1574.
[100] J. H. Shendkar, V. V. Jadhav, P. V. Shinde, R. S. Mane, and C. Dwyer, Heliyon 4 (2018) e00801.
[101] L. Wang, X. Li, T. Guo, X. Yan, and B. K. Tay, Int. J. Hydrogen Energy 39 (2014) 7876.
[102] M. Aghazadeh, Anal. Bioanal. Electrochem. 10 (2018) 554.
[103] M. Li, R. Jijie, A. Barras, P. Roussel, S. Szunerits, and R. Boukherroub, Electrochim. Acta (2019) https://doi.org/10.1016/j.electacta.2019.01.187
[104] C. Jiang, B. Zhan, C. Li, W. Huang, and X. Dong, RSC Adv. 4 (2014) 18080.
[105] G. W. Yang, and C. L. Xu, Chem. Commun. (2008) 6537.
[106] X. Wang, J. Liu, Y. Wang, C. Zhao, and W. Zheng, Mater. Res. Bull. 52 (2014) 89.
[107] G. Wang, L. Zhang, and J. Zhang, Chem. Soc. Rev. 41 (2012) 797.
[108] K. Adib, M. Rahimi-Nasrabadi, Z. Rezvani, S.M. Pourmortazavi, and F. Ahmadi, J. Mater. Sci. Mater. Electron. 27 (2016) 4541.
[109] M. Aghazadeh, H. M. Shiri, and A. A. M. Barmi, Appl. Surf. Sci. 273 (2013) 237.
[110] S. H. Kazem, and A. Asghari, Mater. Lett. 142 (2015) 156.
[111] N. C. Maile, S. K. Shinde, R. R. Koli, A. V. Fulari, D. Y. Kim, and V. J. Fulari, Ultrason. Sonochem. 51 (2019) 49.
[112] M. Aghazadeh, and S. Dalvand, J. Electrochem. Soci. 161 (2014) D18.
[113] C. Chen, M. Cho, and Y. Lee, J. Mater. Sci. 50 (2015) 6491.

[114] A. A. M. Barmi, M. Aghazadeh, B. Arhami, H. M. Shiri, A. A. Fazl, and E. Jangju, Chem. Phys. Lett. 541(2012) 65.
[115] M. Aghazadeh, A. A. M. Barmi, and T. Yousefi, J. Iranian Chem. Soc. 9 (2012) 225.
[116] R. Della Noce, S. Eugenio, T. M. Silva, M. J. Carmezim, and M. F. Montemor, J. Power Sour. 288 (2015) 234.
[117] M. Aghazadeh, A. A. M. Barmi, D. Gharailou, M. H. Peyrovi, and B. Sabour, Appl. Surf. Sci. 283 (2013) 871.
[118] L. Jiang, Y. Sui, J. Qi, Y. Chang, Y. He, F. Wei, Q. Meng, and Z. Sun, Micro Nano Lett. 11 (2016) 837.
[119] M. Aghazadeh, S. Dalvand, and M. Hosseinifard, Ceram. Int. 40 (2014) 3485.
[120] J. Yin, H. U. Lee, and J. Y. Park, RSC Adv. 6 (2016) 34801.
[121] M. Aghazadeh, M. R. Ganjali, and M. G. Maragheh, Int. J. Electrochem. Sci. 12 (2017) 5792.
[122] T. Nguyen, M. Boudard, M. Joaeo Carmezim, and M. F. Montemor, Energy 126 (2017) 208.
[123] M. Aghazadeh, I. Karimzadeh, A. Ahmadi, and M. R. Ganjali, J. Mater. Sci. Mater. Electron. 29 (2018) 14567.
[124] M. Aghazadeh, I. Karimzadeh, A. Ahmadi, M. R. Ganjali, and P. Norouzi, J. Mater. Sci. Mater. Electron. 29 (2018) 14378.
[125] C. Zhao, X. Wang, Sh. Wang, Y. Wang, Y. Zhao, and W. Zheng, Inter. J. Hydrogen Energy. 37 (2012) 11846.
[126] M. Aghazadeh, and M. R. Ganjali, J. Mater. Sci. Mater. Electron. 28 (2017) 11406.
[127] M. Aghazadeh, A. Rashidi, and M. R. Ganjali, Electron. Mater. Let. 14 (2018) 37.
[128] J. H. Shendkar, M. Zate, K. Tehare, V. V. Jadhav, R. S. Mane, M. Naushad, J. M. Yun, and K. H. Kim, Mater. Chem. Phy. 180 (2016) 226.
[129] Q. Cheng, J. Tang, N. Shinya, and L. Qin, Sci. Technol. Adv. Mater. 15 (2014) 014206.
[130] M. Suksomboon, P. Srimuk, A. Krittayavathananon, S. Luanwuthi, and M. Sawangphruk, RSC Adv. 4 (2014) 56876.
[131] X. Xia, J. Tu, Y. Zhang, J. Chen, X. Wang, Ch. Gu, C. Guan, J. Luo, and H. J. Fan, Chem. Mater. 24 (2012) 3793.
[132] J. H. Zhong, A. L. Wang, G. R. Li, J. W. Wang, Y. N. Ou, and Y. X. Tong, J. Mater. Chem. 22 (2012) 5656.
[133] M. J. Deng, C. Song, Ch. Ch. Wang, Y. Ch. Tseng, J. M. Chen, and K. T. Lu, ACS Appl. Mater. Interfaces 7 (2015) 9147.
[134] T. Zhao, H. Jiang, and J. Ma, J. Power Sour. 196 (2011) 860.
[135] J. Zhang, X. Wang, J. Ma, Sh. Liu, and X. Yi, Electrochim. Acta. 104 (2013) 110.
[136] J. Talat Mehrab, M. Aghazadeh, M. G. Maragheh, M. R. Ganjali, and P. Norouzi, Mater. Lett. 184 (2016) 223.

[137] A. Sobhani-Nasab, M. Rahimi-Nasrabadi, H. R. Naderi, V. Pourmohamadian, and M. R. Ganjali, Ultrason. Sonochem. 45 (2018) 189.
[138] M. Naseri, L. Fotouhi, A. Ehsani, and S. Dehghanpour, J. Colloid Interface Sci. 484 (2016) 314.
[139] M. Rahimi-Nasrabadi, V. Pourmohamadian, M. S. Karimi, H. R. Naderi, and M. R. Ganjali, J. Mater. Sci.: Mater. Electron. 28 (2017) 12391.
[140] J. S. Shayeh, A. Ehsani, A. Nikkar, P. Norouzi, M. R. Ganjali, and M. Wojdyla, New J. Chem. 39 (2015) 9454.
[141] J. S. Shayeh, M. Sadeghinia, SOR Siadat, A. Ehsani, M. Rezaei, and M. Omidi, J. Colloid Interface Sci. 496 (2017) 401.
[142] A. Ehsani, J. Khodayari, M. Hadi, and H. M Shiri, Ionics 23 (2017) 131.
[143] M. Rahimi-Nasrabadi, S. M. Pourmortazavi, M. R. Ganjali, and P. Norouzi, J. Mater. Sci.: Mater. Electron. 29 (2018) 2988.
[144] H. M. Shiri, A. Ehsani, and J. S. Shayeh, RSC Adv. 5 (2015) 91062.
[145] Z. J. Han, S. Pineda, A. T. Murdock, D. H. Seo, K. Ostrikov, and A. Bendavid, J. Mater. Chem. A 5 (2017) 17293.
[146] L. Y. Chen, Y. Hou, J. L. Kang, A. Hirata, T. Fujita, and M. W. Chen, Adv. Energy Mater. 3 (2013) 851.
[147] V. D. Patake, C. D. Lokhande, and O. S. Joo, Appl. Surf. Sci. 255 (2009) 4192.
[148] M. Li, and H. He, Appl. Surf. Sci. 439 (2018) 612.
[149] X. Li, and H. He, Appl. Surf. Sci. 470 (2019) 306.
[150] K. H. Kim, K. S. Kim, G. P. Kim, and S. H. Baeck, Curr. Appl. Phys. 12 (2012) 36.
[151] R. K. Vishnu Prataap, R. Arunachalam, R. Pavul Raj, S. Mohan, and L. Peter, Curr. Appl. Phys. 18 (2018) 1143.
[152] K. M. Kim, Y. G. Lee, D. O. Shin, and J. M. Kob, Electrochim. Acta 196 (2016) 309.
[153] B. O. Park, C. D. Lokhande, H. S. Park, K. D. Jung, and O. S. Joo, J. Power Sour. 134 (2004) 148.
[154] M. G. Jeong, K. Zhuo, S. Cherevko, W. J. Kim, and C. H. Chung, J. Power Sour. 244 (2013) 806.
[155] Y. R. Ahn, M. Y. Song, S. M. Jo, C. R. Park, and D. Y. Kim, Nanotechnol. 17 (2006) 2865.
[156] B. O. Park, C. D. Lokhande, H. S. Park, K. D. Jung, and O. S. Joo, J. Mater. Sci. 39 (2004) 4313.
[157] Y. Z. Zheng, H. Y. Ding, and M. L. Zhang, Thin Solid Films 516 (2008) 7381.
[158] J. J. Jhao, C. H. Lin, T. K. Yeh, H. C. Wu, M. C. Tsai, and C. K. Hsieh, Surf. Coat. Technol. 320 (2017) 263.
[159] R. Arunachalam, R. M. Gnanamuthu, M. Al Ahmad, S. Mohan, R. Pavul Raj, J. Maharaja, N. Al Taradeh, and A. Al-Hinai, Surf. Coat. Technol. 276 (2015) 336.

[160] T. M. Dinh, A. Achour, S. Vizireanu, G. Dinescu, L. Nistor, K. Armstrong, D. Guay, and D. Pech, Nano Energy 10 (2014) 288.
[161] C. K. Min, T. B. Wu, W. T. Yang, and C. L. Li, Mater. Chem. Phys. 117 (2009) 70.
[162] S. Cho, J. Kim, Y. Jo, A. T. Aqueel Ahmed, H. S. Chavan, H. Woo, A. I. Inamdar, J. L. Gunjakar, S. M. Pawar, Y. Park, H. Kim, and H. Im, J. Alloys Compd. 725 (2017) 108.
[163] K. C. Ho, and L. Y. Lin, J. Mater. Chem. A (2019) doi: 10.1039/C8TA11599K.
[164] Z. Liu, W. Zhou, S. Wang, W. Du, H. Zhang, C. Ding, Y. Du, and L. Zhu, J. Alloys Compd. 774 (2019) 137.
[165] M. Rahimi-Nasrabadi, H. R. Naderi, M. S. Karimi, and F. Ahmadi, J. Mater. Sci.: Mater. Electron. 28 (2017) 1877.
[166] H. Chen, J. Wang, F. Liao, X. Han, C. Xu, and Y. Zhang, Ceram. Int. (2019) doi:10.1016/j.ceramint.2019.02.010
[167] A. Sobhani-Nasab, H. Naderi, M. Rahimi-Nasrabadi, and M. R. Ganjali, J. Mater. Sci.: Mater. Electron. 28 (2017) 8588.
[168] B. N. Reddy, S. Deshagani, M. Deepa, and P. Ghosal, Chem. Eng. J. 334 (2017) 214.
[169] H. R. Naderi, A. Sobhani-Nasab, M. Rahimi-Nasrabadi, and M. R. Ganjali, Appl. Surf. Sci. 423 (2017) 1025.
[170] F. Liu, H. Su, L. Jin, H. Zhang, X. Chu, and W. Yang, J. Colloid Interface Sci. 505 (2017) 796.
[171] L. Gao, S. Xu, C. Xue, Z. Hai, D. Sun, and Y. Lu, J. Nanoparticle Res. 18 (2016) 1e10.
[172] B. Nor Irwin, S. Z. Sharif Hussein, A. A. Latif, and M. M. Azman, Appl. Mech. Mater. 699 (2015) 181.
[173] M. Aghazadeh, R. Ahmadi, D. Gharailou, M. R. Ganjali, and P. Norouzi, J. Mater. Sci.: Mater. Electron. 27 (2016) 8623.
[174] Y.F. Yuan, X.H. Xia, J.B. Wu, X.H. Huang, Y.B. Pei, J.L. Yang, and S.Y. Guo, Electrochem. Commun. 13 (2011) 1123.
[175] A. D. Jagadale, V. S. Kumbhar, R. N. Bulakhe, and C. D. Lokhande, Energy 64 (2014) 234.
[176] M. Aghazadeh, M. Hosseinifard, B. Sabour, and S. Dalvand, Appl. Surf. Sci. 287 (2013) 187.
[177] J. B. Wu, Y. Lin, X. H. Xi, J. Y. Xu, and Q. Y. Shi, Electrochim. Acta 56 (2011) 7163.
[178] C. W. Kung, H. W. Chen, C. Y. Lin, R. Vittal, and K. C. Ho, J. Power Sources 214 (2012) 91.
[179] M. Aghazadeh, A. Rashidi, P. Norouzi, and M. Ghannadi Maragheh, Int. J. Electrochem. Sci. 11 (2016) 11016.
[180] G. P. Kim, I. Nam, N. D. Kim, J. Park, S. Park, and J. Yi, Electrochem. Commun. 22 (2012) 93.

[181] M. Aghazadeh, J. Appl. Electrochem. 42 (2012) 89.
[182] A. García-Gómez, S. Eugénio, R. G. Duarte, T. M. Silva, M. J. Carmezim, and M. F. Montemor, Appl. Surf. Sci. 382 (2016) 34.
[183] P. Razmjoo, B. Sabour, S. Dalvand, M. Aghazadeh, and M. R. Ganjali, J. Electrochem. Soc. 161 (2014) D293.
[184] X. Zhang, J. Xiao, X. Zhang, Y. Meng, and D. Xiao, Electrochim. Acta 191 (2016) 758
[185] R. Pavul Raja, P. Ragupathy, and S. Mohan, J. Mater. Chem. A 3 (2015) 24338.
[186] R. B. Rakhi, W. Chen, M. N. Hedhili, D. Cha, and H. N. Alshareef, ACS Appl. Mater. Interfaces 6 (2014) 4196.
[187] A. D. Jagadale, V. S. Kumbhar, and C. D. Lokhande, J. Colloid Interface Sci. 406 (2013) 225.
[188] A. García-Gómez, R. G. Duarte, S. Eugénioa, T. M. Silva, M. J. Carmezim, and M. F. Montemor, J. Electroanal. Chem. 755 (2015) 151.
[189] M. Kazazi, A. R. Sedighi, and M. A. Mokhtari, Appl. Surf. Sci. 441(2018) 251.
[190] Y. Fan, H. Shao, J. Wang, L. Liu, J. Zhang, and C. Cao, Chem. Commun. 47 (2011) 3469.
[191] C. Yuan, L. Yang, L. Hou, L. Shen, X. Zhang, and X. W. Lou, Energy Environ. Sci. 5 (2012) 7883.
[192] Y. Zou, I. A. Kinloch, and R. A. W. Dryfe, ACS Appl. Mater. Interfaces 7 (2015) 22831.
[193] V. D. Nithya, and N. Sabari Arul, J. Power Sour. 327 (2016) 297.
[194] N. L. Wu, S. Y. Wang, C. Y. Han, D. S. Wu and L. R. Shiue, J. Power Sour. 113 (2003) 173.
[195] S. Y. Wang, K. C. Ho, S. L. Kuo, and N. L. Wu, J. Electrochem. Soc. 153(2006) A75.
[196] V. D. Nithya, and N. S. Arul, J. Mate. Chem. A. 4 (2016) 10767.
[197] I. Karimzadeh, M. Aghazadeh, M. R. Ganjali, and T. Dourudi, Curr. Nanosci. 13 (2017) 167.
[198] M. Aghazadeh, I. Karimzadeh, and M. R. Ganjali, J. Mate. Sci.: Mater. Electron. 28 (2017) 13532.
[199] M. Aghazadeh, J. Mate. Sci.: Mater. Electron. 28 (2017) 18755.
[200] M. Aghazadeh, and M. R. Ganjali, Ceram. Int. 44 (2018) 520.
[201] M. Aghazadeh, and I. Karimzadeh, Mater. Res. Exp. 4 (2017) 105505.
[202] M. Aghazadeh, I. Karimzadeh, and M. R. Ganjali, J. Mater. Sci.: Mater. Electron. 28 (2017) 19061.
[203] M. Aghazadeh, M. G. Maragheh, and P. Norouzi, Int. J. Electrochem. Sci. 13 (2018) 1355.
[204] M. Aghazadeh, and M. R. Ganjali, J. Mater. Sci. 53 (2018) 295.

[205] M. Aghazadeh, I. Karimzadeh, M. R. Ganjali, and A. Behzad, J. Mater. Sci.: Mater. Electron. 28 (2017) 18121.
[206] M. Aghazadeh, I. Karimzadeh, and M. R. Ganjali, J. Mater. Sci. Mater. Electron. 29 (2018) 5163.
[207] M. Aghazadeh, and M. R. Ganjali, J. Mater. Sci.: Mater. Electron. 29 (2018), 4981.
[208] M. Aghazadeh, I. Karimzadeh, M. G. Maragheh, and M. R. Ganajli, Korean J. Chem. Eng. 35 (2018) 1341.
[209] M. Aghazadeh, I. Karimzadeh, and M. R. Ganjali, J. Electron. Mater. 47 (2018) 3026.
[210] M. Aghazadeh, I. Karimzadeh, and M. R. Ganjali, Phys. Status Solidi A 214 (2017) 1700365.
[211] M. Aghazadeh, I. Karimzadeh, and M. R. Ganjali, Mater. Lett. 209 (2017) 450.
[212] M. Aghazadeh, and M. R. Ganjali, J. Mater. Sci. Mater. Electron. 29 (2018) 2291.
[213] M. Aghazadeh, I. Karimzadeh, M. G. Maragheh, and M. R. Ganajli, Mater. Res. 21 (2018) e20180094.
[214] I. Karimzadeh, Anal. Bioanal. Electrochem. 10 (2018) 338.
[215] M. R. Ganjali, and M. Rezapour, Anal. Bioanal. Electrochem. 10 (2018) 1355.
[216] B. J. Lokhande, R. C. Ambare, R. S. Mane, and S. R. Bharadwaj, Curr. Appl. Phys. 13 (2013) 985.
[217] N. Nagarajan, and I. Zhitomirsky, J. Appl. Electrochem. 36 (2006) 1399.
[218] S. Mitra, P. Poizot, A. Finke, and J. M. Tarascon, Adv. Funct. Mater. 16 (2006) 2281.
[219] K. W. Chung, K. B. Kim, S. H. Han, and H. Lee, Electrochem. Solid-State Lett. 8 (2005) A259.
[220] J. Sun, Y. Huang, C. Fu, Y. Huang, M. Zhu, X. Tao, C. Zhi, and H. Hu, J. Mater. Chem. A 4 (2016) 14877.
[221] M. Aghazadeh, I. Karimzadeh, M. R. Ganjali, and A. Malekinezhad, Int. J. Electrochem. Sci. 12 (2017) 8033.
[222] R. S. Kate, S. A. Khalate, and R. J. Deokate, J. Alloys Compd. 734 (2018) 89.
[223] S. Liu, L. Wang, C. Zheng, Q. Chen, M. Feng, and Y. Yu, ACS Sustainable Chem. Eng. 5 (2017) 9903.
[224] X. Sun, G. Wang, J. Y. Hwang, and J. Lian, J. Mater. Chem. 21 (2011) 16581.
[225] M. S. Wu, Y. P. Lin, C. H. Lin, and J. T. Lee, J. Mater. Chem. 22 (2012) 2442.
[226] B. Li, M. Zheng, H. Xue, and H. Pang, Inorg. Chem. Front. 3 (2016) 175.
[227] H. Mohammad Shiri, and M. Aghazadeh, J. Electrochem. Soc. 159 (2012) E132.
[228] I. Bouessay, A. Rougier, P. Poizot, J. Moscovici, A. Michalowicz, and J. M. Tarascon, Electrochim. Acta 50 (2005) 3737.
[229] I. A. Dhole, S. T. Navale, Y. H. Navale, Y. M. Jadhav, C. S. Pawar, S. S. Suryavanshi, and V. B. Patil, J. Mater. Sci.: Mater. Electron. 28 (2017) 10819.
[230] M. Aghazadeh, J. Mater. Sci.: Mater. Electron. 28 (2017) 3108.

[231] Z. Zeng, B. Xiao, X. Zhu, J. Zhu, and D. Xiao, and J. Zhu, Ceram. Int. 43 (2017) S633.
[232] X. Dai, D. Chen, H. Fan, Y. Zhong, L. Chang, H. Shao, J. Wang, J. Zhang, and C. Cao, Electrochim. Acta 154 (2015) 128.
[233] T. N. Edison, R. Atchudan, and Y. R. Lee, Electrochim. Acta 283 (2018) 1609.
[234] A. Barani, M. Aghazadeh, M. R. Ganjali, B. Sabour, A. A. Malek Barmi, and S. Dalvand, Mater. Sci. Semiconduct. Process. 23(2014) 85.
[235] S. Shahrokhian, R. Mohammadi, and E. Asadian, Int. J. Hydrogen Energy 41 (2016) 17496.
[236] S. T. Navale, V. V. Mali, S. A. Pawar, R. S. Mane, M. Naushad, F. J. Stadlerd, and V. B. Patil, RSC Adv. 5 (2015) 51961.
[237] G. Du, Z. Zeng, B. Xiao, D. Wang, Y. Yuan, X. Zhu, and J. Zhu, Dalton Trans. 46 (2017) 16532.
[238] V. S. Kumbhar, M. H. Cho, J. Lee, W. K. Kim, M. Lee, Y. R. Lee, and J. J. Shim, New J. Chem. 41 (2017) 10584.
[239] M. Aghazadeh, A. Rashidi, M. R. Ganjali, and M. Ghannadi Maragheh, Int. J. Electrochem. Sci. 11 (2016) 11002.
[240] M. Aghazadeh, and M. R. Ganjali, J. Mater. Sci.: Mater. Electron. 28 (2017) 8144.
[241] H. Y. Wu, and H. W. Wang, Int. J. Electrochem. Sci. 7 (2012) 4405.
[242] W. Liu, C. Lu, X. Wang, K. Liang, and B. K. Tay, J. Mater. Chem. A 3 (2015) 624.
[243] J. Zhang, X. Yi, X. C. Wang, J. Ma, S. Liu, and X. J. Wang, J. Mater. Sci.: Mater. Electron. 26 (2015) 7901.
[244] F. Su, X. Lv, and M. Miao, Small 11 (2015) 854.
[245] M. Huang, F. Li, F. Dong, Y. Xin Zhang, and L. L. Zhang, J. Mater. Chem. A 3 (2015) 21380.
[246] Q. Z. Zhang, D. Zhang, Z. C. Miao, X. L. Zhang, and S. L. Chou, Small. 24 (2018) e1702883.
[247] J. G. Wang, F. Kang, and B. Wei, Progress in Mater. Sci. 74 (2015) 51.
[248] W. Wei, X. Cui, W. Chen, and D. G. Ivey, Chem. Soc. Rev. 40 (2011) 1697.
[249] Z. Wang, Q. Qin, W. Xu, J. Yan, and Y. Wu, ACS Appl. Mater. Interfaces 8 (2016) 18078.
[250] Y. Wang, H. Liu, X. Sun, and I. Zhitomirsky, Scripta Mater. 61 (2009) 1079.
[251] T. Yousefi, A. N. Golikand, M. H. Mashhadizadeh, and M. Aghazadeh, J. Taiwan Institute Chem. Eng. 43 (2012) 614.
[252] T. Yousefi, A. N. Golikand, M. H. Mashhadizadeh, and M. Aghazadeh, J. Solid State Chem. 190 (2012) 202.
[253] Y. Wang, S. Dong, X. Wu, and M. Li, J. Electrochem. Soc. 164 (2017) H56.
[254] T. Nguyen, M. J. Carmezim, M. Boudard, and M. F. Montemor, Int. J. Hydrogen Energy 40 (2015) 16355.

[255] J. Tizfahm, M. Aghazadeh, M. G. Maragheh, M. R. Ganjali, and P. Norouzi, F. Faridbod, Mater. Lett. 167 (2016) 153.
[256] M. Aghazadeh, M. R. Ganjali, and P. Noruzi, Thin Solid Films 634 (2017) 24.
[257] J. Hao, W. Li, X. Zuo, D. Zheng, X. Liang, Y. Qiang, B. Tan, B. Xiang, and X. Zou, J. Mater. Sci. 54 (2019) 625.
[258] Y. Z. Gong, J. Tang, C. Zhu, W. Cheng, Z. Jiang, and J. Ma, J. Mater. Sci. Mater. Electron. (2019) DOI:10.1007/s10854-017-7689-5.
[259] M. Aghazadeh, A. Bahrami-Samani, D. Gharailou, and M. Ghannadi Maragheh, J. Mater. Sci.: Mater. Electron. 27 (2016) 11192.
[260] L. K. Wu, J. Xia, G. Y. Hou, H. Z. Cao, Y. P. Tang, and G. Q. Zheng, Electrochim. Acta 191 (2016) 375.
[261] T. Nguyen, M. Boudard, M. J. Carmezim, and M. F. Montemor, Electrochim. Acta 202 (2016) 166.
[262] M. Aghazadeh, M. G. Maragheh, M. R. Ganjali, P. Norouzi, and F. Faridbod, Appl. Surf. Sci. 364 (2016) 141.
[263] M. Aghazadeh, M. Asadi, M. G. Maragheh, M. R. Ganjali, P. Norouzi, and F. Faridbod, Appl. Surf. Sci. 364 (2016) 726.
[264] M. Aghazadeh, M. R. Ganjali, and P. Norouzi, J. Mater. Sci.: Mater. Electron. 27 (2016) 7707.
[265] Y. Wang, and I. Zhitomirsky, Mater. Lett. 65 (2011) 1759.
[266] M. Aghazadeh, M. R. Ganjali, and M. G. Maragheh, Int. J. Electrochem. Sci. 13 (2018) 1161.
[267] M. Aghazadeh, M. Ghannadi Maragheh, M. R. Ganjali, and P. Norouzi, RSC Adv. 6 (2016) 10442.
[268] M. Aghazadeh, J. New Mater. Electrochem. Systems 21 (2018) 133.
[269] R. Cheraghali, and M. Aghazadeh, Anal. Bioanal. Electrochem. 8 (2016) 193.
[270] Rusi, and S. R. Majid, Scientific Reports 5 (2015) 16195.
[271] T. Beyazay, F. E. Sarac Oztuna, and U. Unal, Electrochim. Acta 296 (2019) 916.
[272] C. Xue, Y. Hao, Q. Luan, E. Wang, X. Ma, and X. Hao, Electrochim. Acta 296 (2019) 94.
[273] H.Z. Chi, Y. Q. Wu, Y. K. Shen, C. Zhang, Q. Xiong, and H. Qin, Electrochim. Acta 289 (2018) 158.
[274] F. E. Sarac, U. Unal, Electrochim. Acta 178 (2015) 199.
[275] Y. Jin, H. Chen, M. Chen, N. Liu, and Q. Li, ACS Appl. Mater. Interfaces 5 (2013) 3408.
[276] M. Li, and H. G. Park, Electrochim. Acta 296 (2019) 676.
[277] M. Aghazadeh, Anal. Bioanal. Electrochem. 10 (2018) 961.
[278] H. Gao, F. Xiao, C. B. Ching, and H. Duan, ACS Appl. Mater. Interfaces 4 (2012) 2801.

[279] Q. Cheng, J. Tang, J. Ma, H. Zhang, N. Shinya, and L. C. Qin, Carbon 49 (2011) 2917.
[280] S. L. Chou, J. Z. Wang, S. Y. Chew, H. K. Liu, and S. X. Dou, Electrochem. Commun. 10 (2008) 1724.
[281] P. Lv, P. Zhang, Y. Feng, Y. Li, and W. Feng, Electrochim. Acta 78 (2012) 515.
[282] J. Yang, L. Lian, H. Ruan, F. Xie, and M. Wei, Electrochim. Acta 136 (2014) 189
[283] Z. Bai, H. Li, M. Li, C. Li, X. Wang, C. Qu, and B. Yang, Int. J. Hydrogen Energy 40 (2015) 16306.
[284] K. H. Ye, Z. Q. Liu, C. W. Xu, N. Li, Y. B. Chen, and Y. Z. Su, Inorg. Chem. Commun. 30 (2013) 1.
[285] C. Zhu, S. Guo, Y. Fang, L. Han, E. Wang, and S. Dong, Nano Res. 4 (2011) 648.
[286] Y. Q. Zhao, D. D. Zhao, P. Y. Tang, Y. M. Wang, C. L. Xu, and H. L. Li, Mater. Lett. 76 (2012) 127.
[287] G. Yu, L. Hu, M. Vosgueritchian, H. Wang, X. Xie, J. R. McDonough, X. Cui, Y. Cui, and Z. Bao, Nano Lett. 11 (2011) 2905.
[288] R. Liu, and S. B. Lee, J. Am. Chem. Soc. 130 (2008) 2942.
[289] L. Zhang, T. Li, X. Ji, Z. Zhang, W. Yang, J. Gao, H. Li, C. Xiong, and A. Dang, Electrochim. Acta 252 (2017) 306.
[290] Y. He, W. Chen, X. Li, Z. Zhang, J. Fu, C. Zhao, and E. Xie, ACS Nano 7 (2013) 174.
[291] S. H. Kazemi, M. A. Kiani, M. Ghaemmaghami, and H. Kazemi, Electrochim. Acta 197 (2016) 107.
[292] Y. C. Tsai, W. D. Yang, K. C. Lee, and C. M. Huang, Mater. 9 (2016) 246.
[293] Y. Zhang, L. Li, H. Su, W. Huang, and X. Dong, J. Mater. Chem. A 3 (2015) 43.
[294] Q. Yang, Z. Li, R. Zhang, L. Zhou, M. Shao, and M. Wei, Nano Energy 41 (2017) 408.
[295] A. Sobhani-Nasab, M. Rahimi-Nasrabadi, H. R. Naderi, and V. Pourmohamadian, Ultrason. Sonochem. 45 (2018) 189.
[296] Y. F. Zhang, M. Z. Ma, J. Yang, H. Q. Su, W. Huang, and X. C. Dong, Nanoscale 6 (2014) 4303.
[297] S. Faraji, and F. Nasir Ani, J. Power Sour. 263 (2014) 338.
[298] Y. Wang, J. Guo, T. Wang, J. Shao, D. Wang, and Y. W. Yang, Nanomater. 5 (2015) 1667.
[299] D. Chen, Q. Wang, R. Wang, and G. Shen, J. Mater. Chem. A 3 (2015) 10158.
[300] Y. Li, X. Han, T. Yi, Y. He, and X. Li, J. Energy Chem. (2018) doi:10.1016/j.jechem.2018.05.010
[301] D. Yan, W. Wang, X. Luo, C. Chen, Y. Zeng, and Z. Zhu, Chem. Eng. J. 334 (2018) 864.
[302] S. K. Chang, Z. Zainal, K. B. Tan, N. Azah Yusof, W. M. D. Wan Yusoff, and S. R. S. Prabaharan, Ceram. Int. 41 (2015) 1.
[303] X. Xiao, G. Wang, M. Zhang, Z. Wang, R. Zhao, and Y. Wang, Ionics 24 (2018) 2435.

[304] R. Wang, and J. Wu, Chapter 5, Metal Oxides in Supercapacitors (2017) 99. Doi:10.1016/B978-0-12-810464-4.00005-X
[305] F. Ahmadi, M. Rahimi-Nasrabadi, A. Fosooni, and M. Daneshmand, J. Mater. Sci.: Mater. Electron.27 (2016) 9514.
[306] C. Hao, S. Zhou, J. Wang, X. Wang, H. Gao, and C. Ge, Ind. Eng. Chem. Res. 57 (2018) 2517.
[307] C. Wu, J. Cai, Q. Zhang, X. Zhou, Y. Zhu, P. K. Shen, and K. Zhang, ACS Appl. Mater. Interfaces 7 (2015) 26512.
[308] L. Merabet, K. Rida, and N. Boukmouche, Ceram. Int. 44 (2018) 11265.
[309] M. Rahimi-Nasrabadi, F. Ahmadi, and M. Eghbali-Arani, J. Mater. Sci.: Mater. Electron. 28 (2017) 2415.
[310] S. S. Selima, M. Khairy, and M. A. Mousa, Ceram. Int. 45 (2019) 6535.
[311] M. Rahimi-Nasrabadi, F. Ahmadi, and A. Fosooni, J. Mater. Sci.: Mater. Electron. 28 (2017) 537.
[312] B. Saravanakumar, S. M. Lakshmi, G. Ravi, V. Ganes, A. Sakunthal, and R. Yuvakkumar, J. Alloys Compd. 723 (2017) 115.
[313] F. Ahmadi, M. Rahimi-Nasrabadi, M.A. Daneshmehr, and M. Eghbali-Arani, J. Mater. Sci.: Mater. Electron. 28 (2017) 14362.
[314] M. Rahimi-Nasrabadi, F. Ahmadi, and M. Eghbali-Arani, J. Mater. Sci.: Mater. Electron. 27 (2016) 13294.
[315] Z. Gao, L. Zhang, J. Chang, Z. Wang, D. Wu, F. Xu, Y. Guo, and K. Jiang, Appl. Surf. Sci. 442 (2018) 138.
[316] C. Wu, L. Chen, X. Lou, M. Ding, and C. Jia, Front. Chem. 6 (2018) 597.
[317] F. Ahmadi, M. Rahimi-Nasrabadi, and M. Eghbali-Arani, J. Mater. Sci.: Mater. Electron. 28 (2017) 5244.
[318] Y. Y. Huang, and L. Y. Lin, ACS Appl. Energy Mater. 1 (2018) 2979.
[319] A. J. Christina Mary, and A. C. Bose, Appl. Surf. Sci. 449 (2018) 105.
[320] K. Vijaya Sankar, and R. Kalai Selvan, Electrochim. Acta 213 (2016) 469.
[321] J. S. Sagu, K. G. U. Wijayantha, and A. A. Tahir, Electrochim. Acta 246 (2017) 870.
[322] H. Hou, G. Xu, S. Tan, and S. Xiang, J. Alloys Compd. 735 (2018) 2205.
[323] M. B. Sassin, C. N. Chervin, D. R. Rolison, J. W. Long, Acc. Chem. Res. 46 (2013) 1062.
[324] S. Sahoo, K. K. Naik, D. J. Late, and C. S. Rout, J. Alloys Compd. 695 (2017) 154.
[325] C. M. Papa, A. J. Cesnik, T. C. Evans, and K. S. Choi, Langmuir 31 (2015) 9502.
[326] M. Mirzaee, and C. Dehghanian, Mater. Res. Bull. 109 (2019) 10.
[327] N. Ghassemi, S. S. Hosseiny Davarani, and H. R. Moazami, J. Mater. Sci.: Mater. Electron. 29 (2018) 12573.
[328] H. Barkhordari, H. Heydari, A. Nosrati, and J. Mohammadi, Ionics 25 (2019) 275.

[329] L. Abbasi, and M. Arvand, Appl. Surf. Sci. 445 (2018) 272.
[330] Rusi and S. R. Majid, Electrochim. Acta 175 (2015) 193.
[331] V. H. Nguyen, and J. J. Shim, J. Power Sour. 273 (2015) 110.
[332] J. Wu, P. Guo, R. Mi, X. Liu, H. Zhang, J. Mei, H. Liu, W. M. Lau, and L. M. Liu, J. Mater. Chem. A 3 (2015) 15331.
[333] G. T. Pan, S. Chong, T. C. K. Yang, and C. M. Huang, Mater. 10 (2017) 370.
[334] Rusi, and S. R. Majid, Electrochim. Acta 138 (2014) 1.
[335] H. Heydari, and M. B. Gholivand, Ionics 23 (2017) 1489.
[336] B. Ameri, S. S. Hosseiny Davarani, H. R. Moazami, and H. Darjazi, J. Alloys Compd. 720 (2017) 408.
[337] C. Yuan, J. Li, L. Hou, X. Zhang, L. Shen, and X. Lou, Adv. Funct. Mater. 22 (2012) 4592.
[338] J. Du, G. Zhou, H. Zhang, C. Cheng, J. Ma, W. Wei, L. Chen, and T. Wang, ACS Appl. Mater. Interfaces 5 (2013) 7405.
[339] Y. Vlamidis, E. Scavetta, M. Giorgetti, N. Sangiorgi, and D. Tonelli, Appl. Clay Sci. 143 (2017) 151.
[340] M. Shao, R. Zhang, Z. Li, M. Wei, D. G. Evans, and X. Duan, New J. Chem. 39 (2015) 2181.
[341] M. Shao, R. Zhang, Z. Li, M. Wei, D. G. Evans, and X. Duan, Chem. Commun. 51 (2015) 15880.
[342] X. Li, D. Du, Y. Zhang, W. Xing, Q. Xue, and Z. Yan, J. Mater. Chem. A 5 (2017) 15460.
[343] M. Zhao, Q. Zhao, B. Li, H. Xu, H. Pang, and C. Chen, Nanoscale 9 (2017) 15206.
[344] M. Yang, H. Cheng, Y. Gu, Z. Sun, J. Hu, L. Cao, F. Lv, M. Li, W. Wang, Z. Wang, S. Wu, H. Liu, and Z. Lu, Nano Res. 8 (2015) 2744.
[345] J. Wu, W. W. Liu, Y. X. Wu, T. C. Wei, D. Geng, J. Mei, H. Liu, W. M. Lau, and L. M. Liu, Electrochim. Acta 203 (2016) 21.
[346] S. B. Kulkarni, A. D. Jagadale, V. S. Kumbhar, R. N. Bulakhe, S. S. Joshi, and C. D. Lokhande, Int. J. Hydrogen Energy 38 (2013) 4046.
[347] B. Xiao, W. Zhu, Z. Li, J. Zhu, X. Zhu, and G. Pezzotti, R. Soc. Open Sci. 5 (2018) 180867.
[348] T. Nguyen, M. Boudard, M. J. Carmezim, and M. Fátima Montemor, Scientific Reports 7 (2017) 39980.